PLASMA PROPELLANT INTERACTIONS: RDX FILMS IN HYDROGEN, ARGON, AND MIXED COMPOSITION PLASMAS

by

Rodney Valliere

A dissertation submitted to the Graduate Faculty of
Auburn University
in partial fulfillment of the
requirements for the Degree of
Doctor of Philosophy

Auburn, Alabama
May 5, 2013

Approved by

Rik Blumenthal, Chair, Associate Professor of Chemistry and Biochemistry
William Charles Neely, Professor of Chemistry and Biochemistry
Christian Goldsmith, Assistant Professor of Chemistry and Biochemistry
German Mills, Associate Professor of Chemistry and Biochemistry

ABSTRACT

The interaction of the components in electrothermal chemical (ETC) ignition have been studied due to its advantages over conventional ignition. In ETC ignition, a piece of polyethylene replaces the primer found in conventional ignition. The plastic is attached to a large capacitor that when high transient current results, due to the high temperature, the plastic dissociates into ions, radicals, electrons, and light. The individual and synergistic effects of these components have been studied and are presented in this dissertation.

Erosion rates of RDX films have been measured under a variety of conditions. Experiments were performed to understand the roles of light, electrons, argon ions, hydrogen ions, and hydrogen radicals. The most significant erosion rate was found in high-energy hydrogen plasmas where the synergistic effect of ions and radicals appeared to be the greatest contributor.

The roles of ions and radicals were investigated further through exposing RDX films to mixed hydrogen-argon plasmas. In theory, if the erosion rate of propellants behaved like semiconductor etching, then the addition of argon to a hydrogen plasma should greatly enhance the erosion rate due to the shear size of the argon ions. This is not observed. As a result, a new mechanism for the decomposition of RDX involving the embedment of hydrogen has been described.

To test the roles of carbon atoms and ions in the plasma generated by ETC ignition, an apparatus was designed to obtain a sample of pure carbon atoms. The design incorporates an arc welder, water-cooled electrodes, graphite rods, and liquid nitrogen

cooled glass. Once turned on, a sample of carbon was obtained under vacuum onto a glass slide. Although the design was successful, the integration of the apparatus to the erosion studies was not attempted.

Using a nebulizing spray technique, RDX particle size was changed under a variety of conditions. When a sample of RDX contains particles that are uniform in size, ignition cannot be achieved due to lack of friction. Ideally, RDX would display a size ratio of 10:1 to allow for jagged edges and hot spot growth. A nebulizer can achieve this optimal ration simply by depositing a film of certain size and by changing a few variables, depositing a film that is ten times larger or smaller. The Scherrer Equation was used to obtain the particle size of RDX measured by x-ray diffraction. Performing a multivariate analysis, using concentration, flow rate, gas flow, and spraying distance as independent variables and particle size as the dependent variable, an equation was determined to account for the change in particle size for RDX. All of this work is preliminary and continues.

ACKNOWLEDGEMENTS

First and foremost I would like to express my appreciation and thanks to my advisor, Dr. Rik Blumenthal, for his guidance and encouragement throughout my studies here at Auburn University. My dissertation would not be possible without his advice and undying devotion to this research. Secondly, I would like to thank my other committee members Dr. William C. Neely, Dr. German Mills, and Dr. Christian R. Goldsmith for their helpful discussions and constructive suggestions to my dissertation. I would also like to express my thanks to Dr. Thomas Albrecht-Schmitt for his guidance. I would also like to thank my former and current lab mates Dr. Aaron Orland, Dr. Tatiana Bormitova, and Huijao Sun for their meaningful discussions and help during my studies. I would also like to extend my thanks to the many friends I have made during this stage of my life. I want to especially express my gratitude to my parents Rod and Judy Valliere and my brother, Craig, for always supporting me throughout my life. And last, but certainly not least, I would like to thank the Department of Chemistry and Biochemistry and the Army Research Office for their monetary support.

Style manual used: American Institute of Physics

Computer software used: Microsoft Word, Microsoft Excel, Microsoft Powerpoint

Table of Contents

List of Figures

CHAPTER 1

INTRODUCTION

1.A. Introduction

Electrothermal chemical (ETC) ignition of propellants is new technology that has several important advantages over conventional ignition, most significantly, a reduced and highly reproducible ignition delay[1] and an ability to compensate bed temperature induced changes in muzzle velocity.[2] ETC ignition uses the high-pressure, atomic plasma produced by the ablative discharge of a large capacitor across a polymer tube to replace conventional primers, such as lead azide or black powder, in the ignition of the propellant. The underlying question in ETC ignition is the fundamental mechanism, or mechanisms, of ignition that results in the beneficial performance of this new technology. Propellants are materials can combust and gasify without the addition of oxygen. They are distinguished from explosives, a more general term, by having combustion rates that increase with increasing pressure.[3] Advanced propellants, such as RDX (1,3,5-Trinitro-1,3,5-triazine), demonstrate a resistance to shock and heat before igniting, particularly when the pressure and temperature are not present in combination.[4] Individually, if ignition of RDX is attempted with a "hammer test," nothing will happen. Likewise, if RDX is merely heated, it will burn slowly. This makes it a safer explosive in that accidental discharges in munitions storage facilities can be avoided. Ignition of advanced propellants requires primers to provide the initial pressure and temperature necessary to begin spontaneous combustion of the propellant.

Early investigations of ETC ignition relied primarily on pressure measurements to quantify the performance as a function of discharge current and voltage.[5,6,7]That work was accompanied by simulations of the plasma pulse emerging from the igniter,[8,9] optical imaging of the igniter pulse,[10] measurement of the pressure and compositional profiles of the pulse[11] and measurements of actual muzzle velocities as a function of discharge conditions and propellant bed temperature.[2] The ETC igniter pulse, which has been calculated to have pressures as high as 33 MPa and temperatures as high as 30,000 K, is an extremely difficult environment to probe. At temperatures above 10,000K, the entropy of dissociation becomes greater than the bond enthalpy of even the strongest chemical bonds and molecules spontaneously dissociate into separate atoms. At temperatures above 20,000K entropy favors the dissociation of valence electrons from the atoms and a dense plasma state is formed. In such an environment high radiation fields are generated, which led to early theories of the mechanism of ETC ignition centered on the radiation field.[12] The focus of this work is the experimental determination of the mechanism by which the propellant is ignited by the plasma pulse of the ETC igniter. The method used is commonly referred to as experimental modeling. In experimental modeling, a complex environment that may be difficult to probe, or probe through, like the plasma pulse emerging from an igniter, is replaced with each of its individual components and combinations of the components that are generated in a manner that is compatible with traditional vacuum probes. In the early 1980's, Winters and Coburn[13] used this approach to show that the etch rate of silicon in fluorine plasmas was not only dependent on physical sputtering (due to the ion flux) and chemical reaction (due to the reactive neutral flux), but, more importantly, the rate depended strongly on a synergy of the two effects,

which together result in an etch rate that is nine times the etch rate of either component individually. With the fundamental understanding that was gleaned from those experiments, it is possible to rationally design an etch process to produce a specific desired feature. Many researchers in the semiconductor etching area consider the Winters and Coburn experiment to be one of the most important discoveries in the area, ranking only behind the discovery of the transistor by Bardeen, Brattain and Shockley.[14] Optical imaging of the emerging plasma pulse and measurements of the density and composition of the pulse have been used to test and confirm the prediction of the simulation results. The investigation of muzzle velocities revealed that the differences in muzzle velocity resulting from the propellant bed temperature can be compensated by a simple adjustment of the total charge on the capacitor.

The plasma pulse emerging from the igniter has been shown to be composed of primarily electrons, hydrogen atoms, hydrogen ions, carbon atoms, carbon ions[8] and light.[15] In this work, the interactions of electrons, hydrogen atoms and ions and light are investigated by monitoring the erosion of sprayed-on RDX films (the model propellant) as they were exposed to a low-pressure electron cyclotron plasma under a variety of plasma conditions. Erosion of the films was recorded on videotape, using a conventional video surveillance camera, and reflected light intensity profiles were obtained through digitization of the video signal. Kinetic analysis was performed by displaying light intensity against time. Different fluxes and combinations of plasma pulse components at the surface the RDX films were achieved by varying plasma conditions, feed gases, and/or shielding of the film. For instance, with a negative bias applied to the sample holder, the film can be selectively exposed to a positive ion flux, while at a positive bias

the film can be exposed to an electron flux, and at a floating potential the film can be exposed to a minimal but equal flux of both charged components. In addition, control of the applied bias provides direct control of the average energy of the impingent species, allowing for the investigation of energy effects during erosion. Using plasmas of inert gases, such as argon, the roles of generic ions, electrons, and light can be investigated in the absence of chemically reactive species. Using hydrogen plasmas, the role of reactive hydrogen atoms, in the presence of ions, electrons and light, can be investigated in the absence of chemically reactive species. Finally, using a sapphire window placed above the film, the effects of light can be investigated, as the window has the dual effects of eliminating the charged particle flux and significantly reducing the neutral flux arriving at the RDX film surface.

The erosion rates of RDX films have been measured during exposure to plasmas under differing applied bias and when shielded by a sapphire window. Comparison of the results of the individual experiments reveals an erosion mechanism that is primarily chemical and which is greatly enhanced by ion flux. Electrons and light (with photon energies below 8.2 eV) are shown not to be important in the rate of erosion of the films.

1.B. Plasmas

The simplest definition of a plasma is a partially ionized gas. This statement may not be fully accurate, but it does provide for a good starting point when discussing plasmas. A plasma is a collection of charged particles within an electric field. Plasma can be confined in a container consisting of strong electric fields. Due to buildup of charge on the walls, the electric fields are strongest at the walls of an insulator. Electrons in plasma have much greater mean free paths than ions. This happens because more electrons than

ions strike the walls. This is a direct result from electrons achieving greater velocities than ions. The length of the mean free path can be determined by:

$$\lambda = \nu_{avg}/z, \quad (1.1)$$

where λ is the mean free path, ν_{avg} is the average velocity, and z is the collision frequency. More electrons than ions hit the wall to create a negative charge. This negatively charged wall then attracts ions and repels electrons. Once a steady-state is reached, the wall no longer has a charge. The charged wall will hold lower energy electrons away while allowing higher energy electrons and positive ions to reach the wall.[16]

1.C. Types of Plasma

Glow discharge plasmas are generated in a cell filled with an inert or molecular gas at low pressure. When there is a potential difference between electrodes in the cell, a plasma is created.[17] From the potential difference, atoms of the gas are ionized and free electrons form.[17,5] The positively charged ions accelerate to the cathode where more electrons are released, which bombard other gas particles, and excitation and ionization occur.[17] The radiative decay of the excited species gives rise to the characteristic light of the plasma.[17] Ionization creates more ions and electrons to continue the process and the plasma becomes self-sustaining.[17] Glow-discharge plasmas are probably the most common plasma; this is the type of plasma generated within fluorescent light tubes.

Capacitively coupled plasmas(CCP) are similar to glow discharge plasmas, but generated with high frequency RF electric fields, typically 13.56 MHz. These differ from glow discharges in that the sheaths are much less intense. CCP may have interior electrodes which are separated by a short distance (a few cm).[18] They may be in contact

with the discharge or they be insulated from it by a dielectric.[18] In the case of insulating chamber walls, outer electrodes, are sometimes used.[18]

"The so-called 'self-bias' is a characteristic feature of this type of plasma. The 'self-bias' is a negative dc potential that develops between the plasma and the powered electrode as a consequence of (i) the use of a coupling capacitor between the rf generator and the powered electrode and (ii) the use of appropriately shaped areas of the (smaller) powered electrode and the (larger) grounded electrode."[18] These are widely used for plasma etching and plasma enhanced chemical vapor deposition.

Inductively coupled plasmas (ICP) are similar to a CCP but the electrode consists of a coil wrapped around the discharge volume of gas that is inductively coupled to the RF energy and the electrons and nuclei are separated by the magnetic field generating a plasma.

Similar to CCP and ICP, wave heated plasmas are typically RF (or microwave). They are, however, heated by electrostatic and electromagnetic means and typically require a coaxial magnetic field for wave propagation.[18] Their frequency is typically 2.45 GHz. Examples are helicon discharge, ion cyclotron resonance (ICR), and electron cyclotron resonance (ECR).

1.C. Plasma Source

Electron cyclotron resonance (ECR) sources were the first commercially available sources to achieve plasma densities above 10^{11} cm^{-3}. ECR is a reference to the orbital motion of free electrons moving along circular magnetic field lines while absorbing microwave energy.

In an ECR source, the free electrons are held in circular orbits in a DC magnetic field with an angular frequency given by:

$$\omega_c = qB/m_e s, \quad (1.2)$$

where q is the charge on an electron, m_e is the mass of an electron, s is time in seconds, and B is the magnetic flux density. If the applied microwave frequency equals the cyclotron frequency, $\omega_c = \omega$, then the energy coupling to the plasma is greatly enhanced, and a plasma will be formed through electron impact ionization. By continually pumping microwave energy into the chamber, the orbiting electrons can be maintained at higher energies than electrons created in capacitively coupled systems. The electrons are also less likely to strike a wall before striking an atom or molecule because they travel in circular orbits instead of straight lines. This gives the ECR the ability to efficiently create ions in much greater numbers and greater electron densities than is possible with capacitively coupled systems. The ions are almost completely non-energetic in relation to the substrate, or sample holder, and therefore, the ion energy is only determined by a small sheath potential and by any independent sample biasing. The major drawback of the ECR system is the difficulty in processing large substrates.[16]

1.D. Chemical Reactions in Plasmas

In the plasma environment, there are two basic families of reactions: electron-molecule reactions, and molecule-molecule/molecule-wall collisions. In electron-molecule reactions, electron impact is responsible for driving the reactions. The temperature of the electrons, however, is closely tied to the type of plasma source used. ECR sources have high densities of charged particles ($\leq 10^{12}$ cm^{-3}) and high temperature electrons (Te = 2-5eV). In capacitively coupled reactors, the density of charged particles

and the electron temperatures are usually much lower. Consequently, the type of reactor used and the type of feed gas used will determine whether electrons or ions drive the chemistry of the plasma. This is an important concept for understanding how reactions are driven in plasmas. Within this context, certain general rules will hold true, such as, in a plasma with more energetic electrons, attachment to form negatively charged species will be less likely than in a plasma with less energetic electrons, and the plasma will contain mostly positive ions and the charge will be balanced by the free electrons. In a plasma with cooler electrons, the formation of negative ions will be more prevalent. In almost all cases, however, the reaction scheme will be started by electron-molecule reactions causing the ionization or dissociation of a large number of species until a steady state condition is reached.[16]

1.E. Energetic Materials

Energetic materials are a class of materials with a high amount of stored chemical energy that can be released rapidly. Typical classes of energetic materials are explosives, pyrotechnic compositions, propellants, and fuels.

RDX is an explosive nitroamine widely used in military and industrial applications. See Figure 1.1. Nomenclature variants include cyclonite, hexogen, T4, cyclotrimethylenetrinitramine, cyclotrimethylene-trinitramine, cyclotrimethylene trinitramine. In its pure, synthesized state RDX is a white, crystalline solid. As an explosive, it is the major component of many formulations, which may vary by the

.

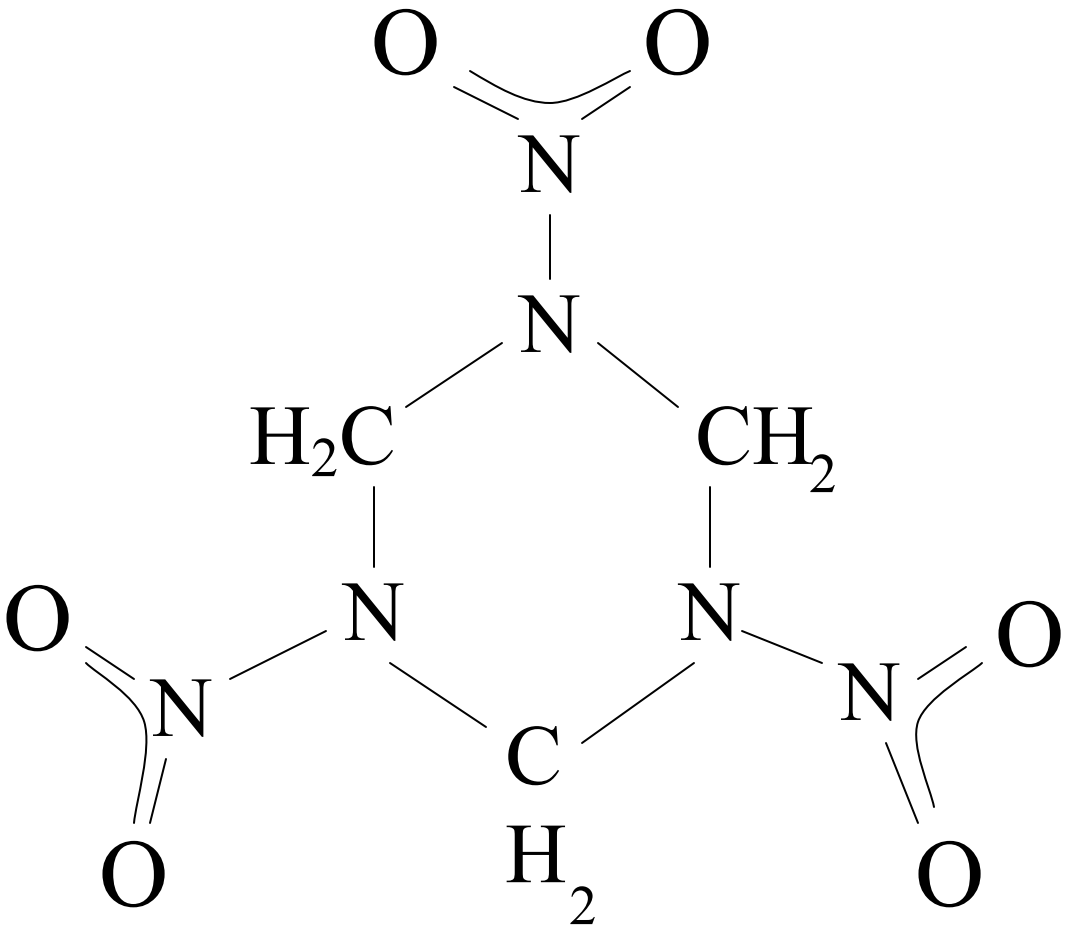

Figure 1.1: Structure of RDX

amount of other explosives and plasticizers, phlegmatizers, or desensitizers. It is stable in storage and is considered one of the most powerful and brisant of the military high explosives. There are many explanations for the name RDX, including (but not limited to) Royal Demolition eXplosive, Research Department (composition) X and Research Department eXplosive. Research Department composition X is most likely correct. In the United Kingdom, new military explosives were given an identification number preceded by the letters 'RD' indicating 'Research Department No.'. For some reason, this explosive was unable to be given a number. Instead, the letter 'X' was appended to indicate 'unknown' with the intention of adding the number later.

RDX was first prepared by Henning for medical use in 1899. It was not used as an explosive until 1920 by Herz[18] who succeeded in directly nitrating hexamine.

$$(CH_2)_6N_4 + 4HNO_3 \rightarrow (CH_2\text{-}N\text{-}NO_2)_3 + 3HCHO + NH_4^+ + NO_3^-$$

His yields, however, were low and the process was too expensive for large-scale production. In 1925, Hale established yields of 68%, but no significant improvements were made to the manufacture until 1940 when Meissner developed a continuous method, and Ross and Scheissler developed a method that did not include hexamine as a starting material.[18] Concurrently, Bachman developed a process that gave the highest yield. His product was known as Type B RDX, which contained 8-12% impurities.[19] From these impurities, another explosive, HMX, was developed. Brockman developed a process to synthesize pure RDX also know as Type A RDX with no impurities.[19] Due to its stability and lower sensitivity, RDX replaced PETN. It was used by both sides in World War II.

The velocity of detonation of RDX at a density of 1.76 g/cm³ is 8750 m/s. It is a colorless solid, of maximum theoretical crystal density 1.82 g/cm³ at 20ºC. It is a heterocycle and has the molecular shape of a ring. It starts to decompose at about 170 °C and melts at 204 °C. Its structural formula is: hexahydro-1,3,5-trinitro-1,3,5-triazine or $(CH_2\text{-}N\text{-}NO_2)_3$. At room temperature, it is very stable. It burns rather than explodes and detonates only with a detonator, being unaffected even by small arms fire. It is less sensitive than pentaerythritol tetranitrate (PETN). However, it is very sensitive when crystallized, below −4 °C.

1.F. Ignition Processes

Shock is a transient physical excitation.[20] A mechanical or physical shock is a sudden acceleration or deceleration caused, for example, by impact, drop, kick, earthquake, or explosion.[20] Primary high explosives may be detonated with mechanical shock or impact.

When gases are compressed, heat is generated, or more accurately, energy is transferred. If the rate of heat generation within a system exceeds the rate of heat loss (energy transfer) to the surroundings, the temperature of the system will rise. If the rate of compression is rapid enough such that the heat loss may be considered negligible, resulting in “adiabatic compression”, the temperature rise will depend on compression ratio.[21] The mathematical equation for an adiabatic process can be written as:

$$pV^{\gamma} = \text{constant} \tag{1.3}$$

where p is the pressure, V is the volume, and

$$\gamma = Cp/Cv \quad (1.4)$$

where Cp is the specific heat at constant pressure and Cv is the specific heat at constant volume.

Diesel engines work on this basic principle The rate of pressure rise is generally relatively slow in snubbing operations. This allows heat (energy) to dissipate to the surroundings. Typical timing for compression to a maximum pressure is in the order of several hours as opposed to a fraction of a second (ms) in diesel engines. Sudden compression, however, may be an ignition source (e.g.when a valve is suddenly opened resulting in the rapid compression of an air-hydrocarbon mixture) and is worth consideration when analyzing snubbing incidents. A compression ratio of 18:1 for air initially at ambient temperature produces temperatures of 674°C, which can ignite dry tinder. A liquid with gas bubbles can also ignite due to rapid compression. Here's why. The volume of gas bubbles will change at a faster rate than the volume of the liquid, resulting in the bubbles becoming hot spots and a potential ignition source.[21]

The size or intensity of arcs and sparks depends on the resistance of the substance between the points of discharge. Once the voltage is high enough to overcome the dielectric strength of the air, the air will ionize allowing a conductive path for electricity to flow. Due to the high resistively of air, there will generally be enough energy dissipated in an arc or spark to ignite a flammable vapor. The current or amount of electricity that is flowing will dictate the temperature of the arc. The higher the current, the higher the temperature.[21]

Sparks are the discharge of electrons that may or may not expend all of the energy in a single discharge. An arc is a continuous stream of electrons bridging a gap between two conductive surfaces in close proximity.[21]

Ignition by mechanical sparks occurs when there is excessive friction between metals or extremely hard substances. As the two substances rub against each other, small particles are torn off the surfaces. This tearing is due to the large amount of friction.[21]

References

[1]A. Chaboki, S. Zelenak, and B. Isle, IEEE Trans. Magn. **33**, 284 (1997).

[2]H. K. Haak, P. Scaffers, T. H. G. G. Weise, and H. G. Wisken, IEEE Trans. Magn. **39**, 231 (1997).

[3]N. Kubota, *Propellants and Explosives: Thermochemical Aspects of Combustion*, 2nd edition, Wiley-VCH Verlag GmbH & Co. KGaA. 208 (2007).

[4]secondary explosive. In *Encyclopædia Britannica*. (2011).

[5] S. Andreasson and M. U. Carlson, IEEE Trans. Magn. **35**, 181 (1999)

[6]R. A. Beyer and R. A. Pesce-Rodriguez, IEEE Trans. Magn. **39**, 207 (2003).

[7]R. A. Fifer, E. S. Sagan, and R. A. Beyer, IEEE Trans. Magn. **39**, 218 (2003).

[8]M. J. Nusca and M. J. McQuaid, CPIA Publ. **691**, 143 (1999).

[9]M. J. Nusca, M. J. McQuaid, and W. A. Anderson, J. Thermophys. Heat Transfer **16**, 157 (2001).

[10]J. M. Kohel, L. K. Su, N. T. Clemens, and P. L. Varghese, IEEE Trans. Magn. **35**, 201(1999).

[11]J. Li, T. A. Litzinger, and S. A. Thynell, J. Propul. Power **21**, 44 (2005).

[12]K. Kappen and R. Beyer, Propellants, Explos., Pyrotech. **28**, 1 (2003).

[13]H. F. Winters and J. W. Coburn, J. Vac. Sci. Technol. B **3**, 1376 (1985).

[14]J. Bardeen and W. H. Brattain, Phys. Rev. **74**, 230 (1947); W. H. Brattain and J. Bardeen, *ibid.* **74**, 231 (1947); W. Shockley and G. L. Pearson, *ibid.* **74**, 232 (1947).

[15]K. Kappen and U. H. Bauder, IEEE Trans. Magn. **35**, 192 (1999).

[16]A.S. Orland, "The Chemical Mechanisms of Metal Etching in High Density Plasmas," (2003).

[17]A. Bogaerts, J. Anal. At. Spectrom., **14**, 1375–1384(1999).

[18]H. Conrads and M. Schmidt, Plasma Sources Sci. Technol. **9,** 441–454(2000).

[19]J. Akhavan, *The Chemistry of Explosives*, 2nd edition, Royal Society of Chemistry. 9-11 (2004).

[20] Cram101, *e-Study Guide for Conceptual Physical Science by Paul Hewitt*, Content Technologies. (2013)

[21] Fire and Explosions in the Canadian Upstream Oil and Gas Industry, WWW document, http://www.firesandexplosions.ca/index.php

CHAPTER TWO

STRONG SYNERGISTIC EFFECTS IN THE COMBUSTION OF PROPELLANTS IN H_2 PLASMAS

2.A. Introduction

Electrothermal chemical (ETC) or plasma ignition of propellants has been investigated by observing the interactions of individual and combinations of the individual components of an ETC pulse with a thin film of propellant. Adjusting the applied dc bias of high-density hydrogen and argon plasmas, ions or electrons may be drawn to the film surface with defined energies and resulting in erosion of the film. Strong synergistic effects are observed between reactive hydrogen atoms and ion bombardment, and a physical model of the process is presented. These synergistic effects may be directly related to the short, highly reproducible ignition delay that characterizes the ETC ignition technology.

ETC ignition of propellants is a technology that has several important advantages over conventional ignition, most significantly, a reduced and highly reproducible ignition delay[1-3] and an ability to compensate bed temperature induced changes in muzzle velocity.[4] ETC ignition uses the high-pressure, atomic plasma produced by the ablative discharge of a large capacitor across a polymer tube to replace conventional primers, such as lead azide or black powder, in the ignition of the propellant. The underlying question in ETC ignition is the fundamental mechanism, or mechanisms, of ignition that results in the beneficial performance of this technology.

Both explosives and propellants are materials that combust and gasify rapidly, resulting in large pressure increases. Propellants, also known as secondary explosives, may be distinguished from traditional, or primary, explosives in that they are not as easily ignited. The advanced propellants, such as 1,3,5-trinitro-1,3,5-triazinane (RDX), demonstrate a high resistance to shock or heat, particularly when the pressure and temperature are not present in combination. Their ignition normally requires the ignition of small charge of primary explosive to provide the initial pressure and temperature necessary for their spontaneous combustion. Consequently, minimizing the amount of primary explosive used, or even eliminating the use of primary explosive completely, can significantly reduce the likelihood of accidental detonations.

Early investigations of ETC ignition relied primarily on pressure measurements to quantify the performance as a function of discharge current and voltage.[5–7] That work was accompanied by simulations of the plasma pulse emerging from the igniter,[8-10] optical imaging of the igniter pulse,[11] measurement of the pressure and compositional profiles of the pulse,[12-14] and measurements of actual muzzle velocities as a function of discharge conditions and propellant bed temperature.[4] The investigation of muzzle velocities revealed that the differences in muzzle velocity resulting from the propellant bed temperature can be compensated by a simple adjustment of the total charge on the capacitor. Optical imaging of the emerging plasma pulse and measurements of the density and composition of the pulse have been used to test and confirm the prediction of the simulation results. The ETC igniter pulse, which has been calculated to have pressures as high as 33 MPa and temperatures as high as 30000 K, is an extremely difficult environment to probe. At temperatures above 10000 K, the entropy of

dissociation becomes greater than the bond enthalpy of even the strongest chemical bonds and molecules spontaneously dissociate into separate atoms. At temperatures above 20000 K, entropy favors the dissociation of valence electrons from the atoms and a dense plasma state is formed. In such an environment, high radiation fields are generated, which led to early theories of the mechanism of ETC ignition centered on the radiation field.[15]

The focus of this work is the experimental determination of the mechanism by which the propellant is ignited by the plasma pulse of the ETC igniter. The method used is commonly referred to as experimental modeling. In experimental modeling, a complex environment that may be difficult to probe, or probe through, like the plasma pulse emerging from an igniter, is replaced with each of its individual components and combinations of the components that are generated in a manner that is compatible with traditional vacuum probes. In the late 1970s, Winters and Coburn[16] used this approach to show that the etch rate of silicon in fluorine plasmas was not only dependent on physical sputtering (due to the ion flux) and chemical reaction (due to the reactive neutral flux) but, more importantly, the rate depended strongly on a synergy of the two effects, which together result in an etch rate that is nine times the etch rate of either component individually. With the fundamental understanding that was gleaned from those experiments, it is now possible to rationally design an etch process to produce a specific desired feature. Many researchers in the semiconductor etching area consider the Winters and Coburn experiment to be one of the most important discoveries in the area, ranking only behind the discovery of the transistor by Bardeen, Brattain, and Shockley.[17]

The plasma pulse emerging from the igniter has been shown to be composed of primarily electrons, hydrogen atoms, hydrogen ions, carbon atoms, carbon ions,[9] and

light.[18] In this work, the interactions of electrons, hydrogen atoms and ions, and light are investigated by monitoring the erosion of sprayed-on RDX films (the model propellant), as they were exposed to a low-pressure electron cyclotron plasma under a variety of plasma conditions. Erosion of the films was recorded on videotape, using a conventional video surveillance camera, and reflected light intensity profiles were obtained through digitization of the video signal, and used in the kinetic analysis. Different fluxes and combinations of plasma pulse components at the surface of the RDX films were achieved by varying plasma conditions, feed gases, and/or shielding of the film. For instance, with a negative bias applied to the sample holder, the film can be selectively exposed to a positive ion flux, while at a positive bias the film can be exposed to an electron flux, and at floating potential the film can be exposed to a minimal but equal flux of both charged components. In addition, controlling the applied bias provides direct control of the average energy of the impingent species, allowing for the investigation of energy effects during erosion. Using plasmas of inert gases, such as argon, the roles of generic ions, electrons, and light can be investigated. Using hydrogen plasmas, the role of reactive hydrogen atoms, in the presence of ions, electrons, and light, can be investigated. Finally, using a sapphire window placed above the film, the effects of light can be investigated, as the window has the dual effects of eliminating the charged particle flux and significantly reducing the neutral flux arriving at the RDX film surface.

The erosion rates of RDX films have been measured during exposure to plasmas under differing applied bias and when shielded by a sapphire window. Comparison of the results of the individual experiments reveals an erosion mechanism that is primarily

chemical and which is greatly enhanced by ion flux. Electrons and light (with photon energies below 8.2 eV) are shown not to be important in the rate of erosion of the films.

2.B. Experimental

All plasmas were generated with an ASTeX 4300 Compact ECR-Microwave Plasma Source, operated at 200W forward power and a gas flow rate of 17 SCCM using a MKS model 1159 gas flow regulator and a model 247C controller. An auxiliary magnet, located outside the chamber and ~ 30 cm downstream of the plasma source, was used to confine the plasma to a cylindrical shape.[19] Concentric rings of RDX were sprayed from 1.0 mg/ml analytic standard solutions in acetonitrile obtained from Cerilliant, as described previously.[19] The RDX is fed through a capillary through a syringe pump. The fast-moving, dry, sheath gas(N_2) desiccates the droplets that emerge from the capillary and carries them along to deposit on the substrate as it is rotated to allow for additional drying time for the residual solvent. Each ring represents ~ 0.1 ml of solution or a total of 0.1 mg of RDX. Figure 2.1 is a sketch of the deposition process.

Video images of the erosion films of RDX were recorded on videotape using a commercial surveillance camera from which the infrared illumination diodes had been removed. In most experiments, the films were illuminated with elliptical spot, E.O. Edmund Model Y52-094 (5.0mW @ 670 nm) diode laser at a glancing incidence, with an E.O. Edmund Model Y43-087 narrow bandpass interference filter (671 nm) in front of the camera lens to maximize the ratio of laser light scattered from the deposited film to background light from the plasma. In the electron impact and sapphire window experiments, illumination at glancing incidence was achieved using a quartz-halogen

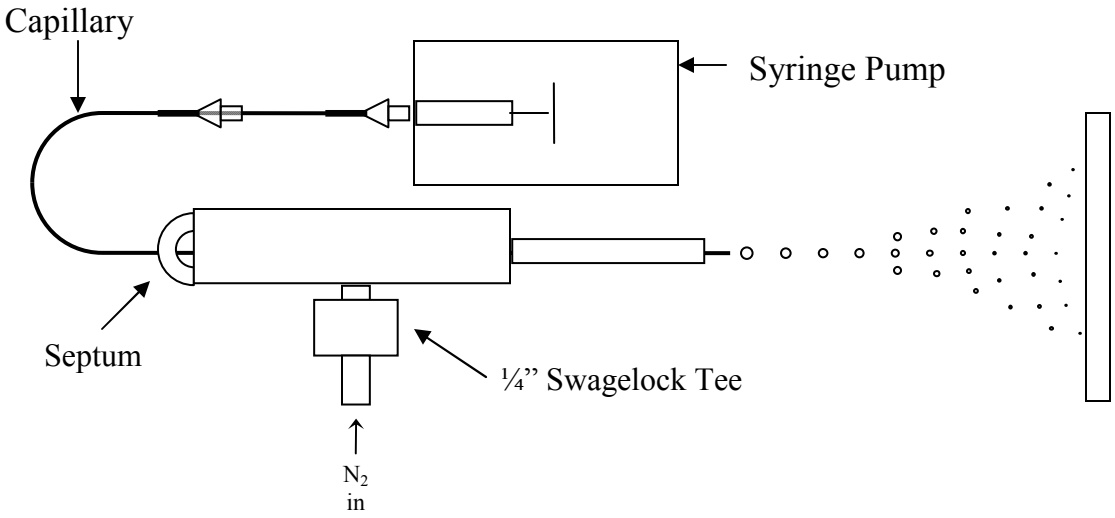

Figure 2.1: Nebulizing Spray Setup

lamp collimated with a horizontal slit placed over the vacuum port window and no filter on the camera was used.

The dc-bias was maintained on the substrate by a KEPCO BOP 1000M bipolar operation amplifier. Application of a negative bias on the sample draws ions from the plasma to the surface and repels electrons form the surface. This results in the generation of a dark region above the surface that grows ~3 mm / 100 V, as the bias is made more negative. Both the thickness of the dark region and the resulting current at the sample surface are functions of the dielectric constant of the plasma, which itself is a function of the degree of ionization of the gas used to generate the plasma. As a result, it is not possible to vary the sample current and bias independently.

A number of tasks were needed to convert the analog video to an Excel file. First, the video was digitized using WinTV. The number of frames was reduced using Fade to Black. Slicer Dicer was used to crop the frames from any unnecessary background imaging. Blaze Media Pro was then used to convert the video format. Finally, Transform was used to convert to an Excel file where ultimately, integration of the intensity around each sprayed-on RDX was performed.

To perform a kinetic analysis, the relationship between the observable (the scattered light intensity) and the amount of material must be developed. The microstructure of sprayed-on RDX films has been previously characterized as a collection of small isolated crystallites with irregular shapes and a relatively narrow distribution of sizes.[20] The principal assumption of the following kinetic analysis is that the scattered light intensity is proportional to the amount of RDX remaining on the substrate. Numerous arguments can be made to support a variety of non-linear

relationships between the scattered light intensity and the amount of RDX remaining on the surface, but they are not justified by the data, see below, which is consistent with a simple linear relationship.

Another simplifying assumption of the kinetic analysis is the use of first order kinetics, which is also shown below to be fully consistent with the data, see below. The equation for first order kinetics is

$$Rate_{Erosion} = - \ d[RDX]/dt = k * [RDX], \quad (2.1)$$

where $Rate_{Erosion}$ is the measured rate of erosion or reaction, k is the rate constant for the process and [RDX] represents the amount of RDX or concentration of RDX crystallites on the surface. The solution of the first order rate differential equation (2.1) assuming a linear relationship between scattered light intensity and the amount of RDX on the surface is

$$\ln([RDX]_t/[RDX]_0) = -kt \quad (2.2)$$

which becomes

$$\ln(I_t/I_0) = -k_{eff}t \quad (2.3)$$

where $[RDX]_t$ is the amount of RDX on the surface at time t, $[RDX]_t$ is the initial amount of RDX on the surface, I_t is the scattered light intensity at time t and I_0 is the initial scattered light intensity. The effective first order rate constant, k_{eff} can be determined directly as the slope of a normalized plot of the natural logarithm of scattered light versus time. Since the same amount of RDX is used in all of the rings, the k_{eff} of different experiments may be compared directly regardless of differences in lighting conditions or variation in the amount of RDX in each ring.

2.C. Results

The erosion of a RDX film under exposure to an argon plasma as the plasma conditions are adjusted is shown in Figure 2.2. For the initial 200 s, the sample was at floating potential, ~ -15 V. At 200 s, the applied bias was set to 0 V, which was then maintained for 300 s. The applied bias was then decreased in steps of 300 V for each 300 s. After the −900 V exposure, H_2 was added and the bias maintained at −900 V to completely remove the film and establish a base line light level. It is clear from the data that exposure to the plasma under negative bias conditions results in erosion of the film.

Figure 2.2 is a plot of the natural logarithm of scattered light intensity versus time. The linear response within each region of constant applied bias indicates that the assumptions of first-order kinetic and a linear relationship between the scattered light intensity and the erosion rate are both reasonable. The different slopes observed at different applied biases indicate that the rate constants are also a function of ion energy. A few features of the data are worth noting. In the initial 100 s under −300 V applied bias, a greater slope is observed than is observed in the second 200 s. This anomalously fast erosion of the film is a common feature of virtually all experiments during the initial period of large negative bias. Second, a significant etch rate is observed at the floating potential where small but equal ion and electron currents exist. Finally, at 0 V applied bias, where a small electron current results, an etch rate that is nearly zero is observed, which indicates a negligible erosion rate.

The inset of the figure is a plot of the effective rate constants, k_{eff}, as a function of bias. Consistent with the comments above about the −300 V applied bias region, the slope in that region was based on only the second 100 s. For pure sputtering, the sputter yield should follow the form,[21]

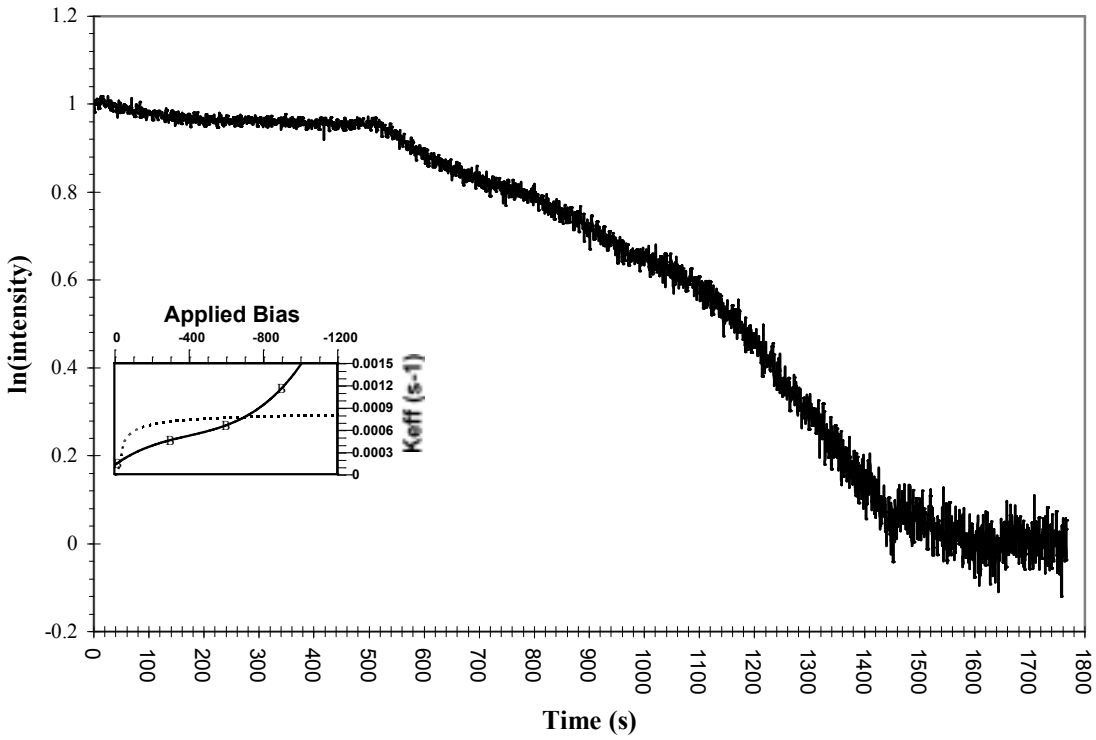

Figure 2.2: Erosion of RDX in Ar Plasmas under different voltages

$$Y(E) = Y_0[1 - (E_{th}/E)^{1/2}], \quad (2.4)$$

where Y_0 is the Sigmund sputter yield and E_{th} is the threshold energy for sputtering. The dashed curve in the inset represents a best fit to that formula. It is obvious that the data are not consistent with the standard sputtering model. Equally important, significant erosion is observed at the floating potential, ~ -15 V, while the expected threshold for sputtering is typically 40–50 eV. The only logical conclusion is that the process of erosion under ion bombardment in argon plasmas is not simple sputtering. In addition, the erosion rate cannot be attributed to photon irradiation from the plasma, since the plasma does not even go dim at 0 V, where virtually no erosion is observed in the presence of light. One possibility is that the observed erosion rate in argon plasmas is a chemically enhanced sputtering process, where the initial ion impact triggers the exothermic decomposition of one, or more, near surface RDX molecules. The chemical enhancement may occur as the heat and/or escaping gases from the initial impact cause additional nearby molecules to decompose, sublime, or simply be physically ejected from the surface.

Erosion experiments carried out under electron impact conditions in argon plasmas, with positive applied bias up to +200 V, produced little observable film erosion over the 2 hour time span of the videotape used to record the data. Hence, it may be concluded that erosion due to electron impact and light is negligible.

Exposure of RDX films to hydrogen plasmas entails several significant differences when compared to argon plasmas. Among these are the generation of chemically reactive hydrogen atoms, a significantly lower average ion mass, a different degree of ionization, and a different emission spectrum. The dissociation of hydrogen

molecules to generate reactive hydrogen atoms opens the possibility of an additional chemical channel leading to the combustion of the RDX. The lower mass of hydrogen compared to argon atoms indicates that erosion due to physically sputtering should be far less in hydrogen plasmas. The degree of ionization also should be expected to differ between argon and hydrogen plasmas. The ionization potentials of argon, hydrogen molecules, and hydrogen atoms are 15.76, 15.43, and 13.60 eV, respectively. As a consequence, hydrogen plasmas should be expected to have a higher density of ions (primarily atomic) and free electrons than argon plasmas. The greater degree of ionization is consistent with the observation that hydrogen plasmas are brighter than equivalent argon plasmas.

The erosion of RDX films in hydrogen and argon plasmas under a floating potential, 0 V applied bias, and under −800 V applied bias is shown in Figure 2.3. The most striking feature of the plot is the very rapid erosion of the film in the hydrogen plasma under the −800 V bias. In the hydrogen plasma, all of the film remaining when the −800 V bias is applied is eroded in less than 100 s, while it takes ~ 800 s to erode an equivalent amount of material in the argon plasma. Also of note is the fact that the rate of erosion at 0 V applied bias in hydrogen plasmas is much greater than the rate in comparable argon plasmas. The jumps observed in the hydrogen plasma data when the 0 V bias is applied and halfway through the 0 V bias region are the result of changes in the brightness of the plasma, exaggerated by the presence of an intense hydrogen emission line close to the bandpass of the notch filter for the illumination laser.

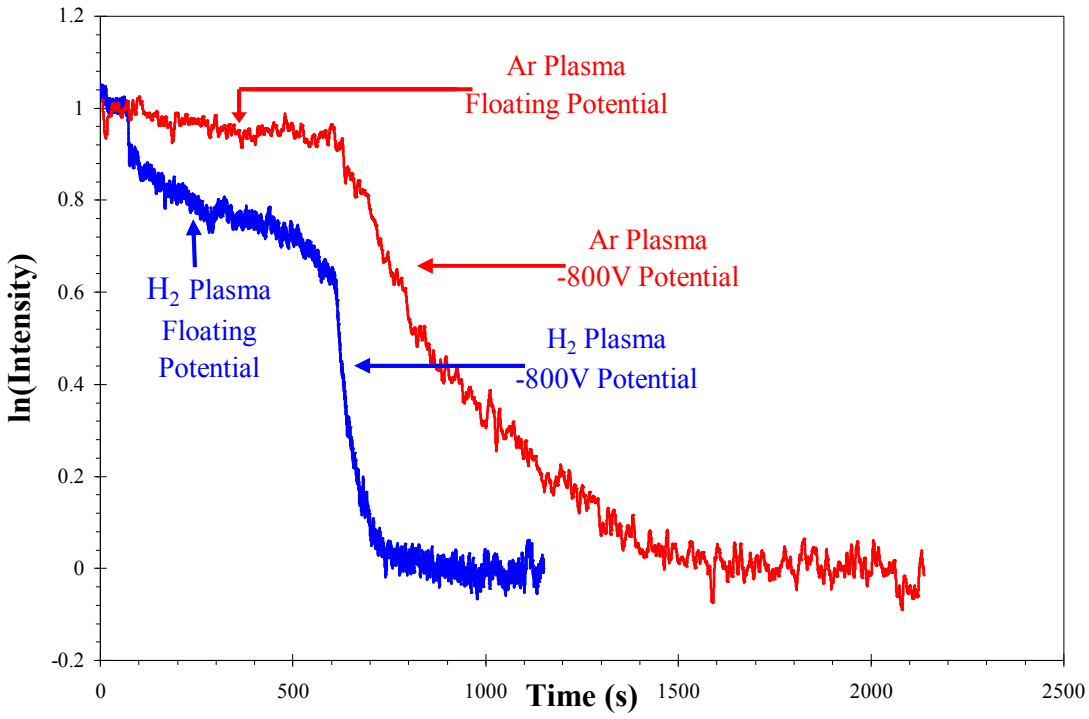

Figure 2.3: RDX Erosion Rates in Ar and H_2 plasmas under the same conditions

If physical sputtering were the major mechanism of erosion, one would expect that the rate of erosion in the argon plasmas to be larger by a factor of 4.5, assuming molecular hydrogen ions, or 6.3, assuming atomic hydrogen ions, based on the square root of the mass ratios. The data show the exact opposite trend. The effective rate constants obtained from the slopes of the natural logarithms of the intensities are 6.5×10^{-4} and 9.2×10^{-5} s^{-1} for the hydrogen and argon plasmas at 0 V applied bias, respectively, and 2.1×10^{-2} and 2.7×10^{-3} s^{-1} for the hydrogen and argon plasmas at −800 V applied bias, respectively. In both cases, the rate of erosion was higher in the hydrogen plasmas by a factor of 7, and the enhancement in the presence of ion bombardment is a factor of 30. Considering that the mass ratios of hydrogen and argon ions, the observed erosion rate in hydrogen plasmas is on the order of 35-fold greater than that predicted by physical sputtering.

Unfortunately, the experimental design does not provide for the independent control of bias and sample current. However, by adjusting the current on the confinement magnet, i.e., adjusting the coupling of the microwave power to the plasma, it is possible to obtain different ion currents at a given applied bias. Figure 2.4 is a plot of the natural logarithm of the scattered light intensity as a function of time as a RDX film was exposed to a hydrogen plasma at 0 and −700 V applied biases with two different power coupling conditions. In the initial period, the erosion rate appears linear over some regions and fluctuates in others. This phenomenon is commonly observed in plasmas where the power coupling has not been optimized. It is presumed to result from a nonlinear response of plasma brightness to small changes in confinement magnet current. In the second period, the film was exposed to a −700 V applied bias that yielded an ion current

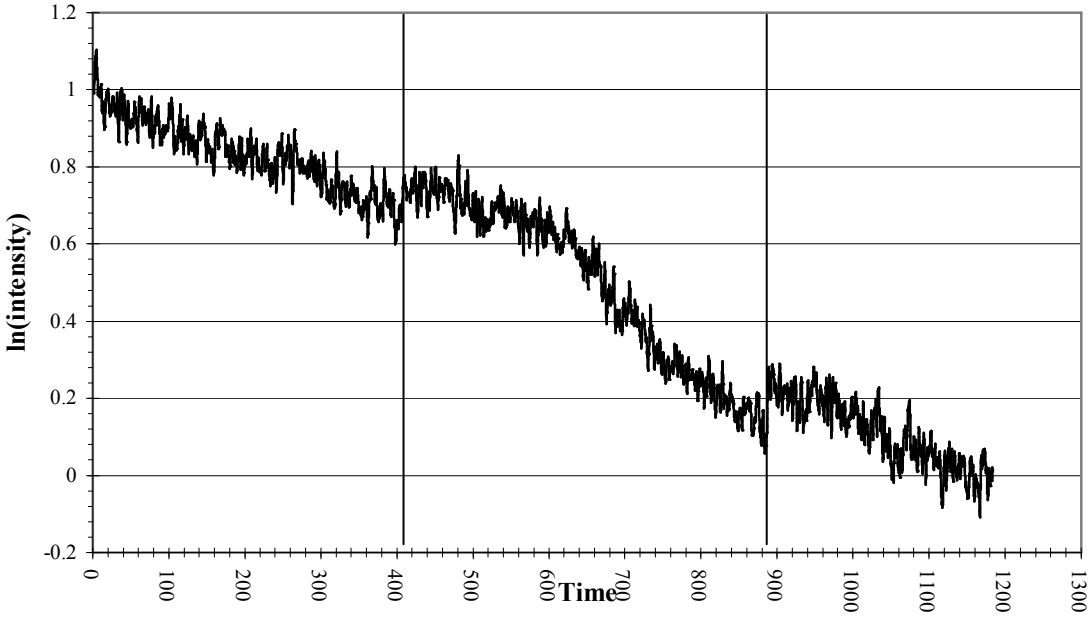

Figure 2.4: RDX exposed to a hydrogen plasma with the same voltage, but different ion currents

of 10.6 mA. In the final period, the confinement magnet current was adjusted to yield an optimized plasma with an ion current of 20.0 mA. The jump at the transition between the second and third periods is due to an increase in a hydrogen atom emission line that overlaps the wavelength of the laser and filter. It is quite apparent that the rate of erosion does not increase linearly with increasing ion current. In fact, upon doubling of the ion current at fixed bias, the rate constant for erosion (based on the time periods of 730–880 s and 900–1100 s) actually decreases by 32%. It is important to note that at other large, negative biases similar results are obtained, when the current is doubled by initially failing to optimize the power coupling.

Based on the results shown in Figure 2.3, there is no question that ion bombardment increases the rate of erosion over the rate observed in the absence of ion bombardment. However, based on Figure 2.4, it is equally clear that the relationship between the erosion rate and the ion bombardment current is not simple. As mentioned above and as seen in the data, changing the confinement current affects more than just the ion current. It is obvious that the light emission also changes and it would be expected that the degree of dissociation and, consequently, the flux of reactive hydrogen atoms to the surface will also be affected. As a result, quantitative comparisons of erosion rates in plasmas with different power coupling conditions are not justified.

To further investigate the role of energetic ions in the erosion of propellant films in hydrogen plasmas, the erosion rates have been measured as a function of decreasing negative bias. With the higher rates of erosion in hydrogen plasmas, it is not possible to measure multiple rates in one experiment as was done in the argon plasmas. The erosion

data of four different films at −500, −600, −800, and −1000 V applied biases are plotted in Figure 2.5. It is clear that the rate of erosion increases with increasing negative bias. The bias dependence of the resulting first-order rate constants is shown in the inset. The dashed line in the inset represents the best fit to the theoretical yield. The applied bias dependence of the erosion rate of RDX in hydrogen plasmas clearly does not resemble the theoretical curve, which rises rapidly over the initial 100 V of bias and then levels off. Instead, erosion in hydrogen plasmas rises significantly with increasing negative bias, indicating a strong synergistic interaction between ions and reactive radicals. The major enhancement in the erosion rate is believed to be the result of implantation of hydrogen ions below the surface that then act to initiate subsurface decomposition of the RDX. The details of the proposed mechanism are discussed in depth in the Discussion section, below.

Erosion of RDX films under electron impact conditions has been measured as a function of positive sample bias in hydrogen plasmas. Figure 2.6 is a plot of the RDX film exposed to a hydrogen plasma with the applied potential alternated between the floating potential, −15 V, and increasing positive biases. The jumps between the periods of applied bias result from significant changes in light emission from the plasma reaching the camera, which was operated with no filter and quartz lamp illumination. The similar slopes of the curves under all of the bias conditions examined indicate that the rate of erosion does not change drastically between any of the bias conditions. Differences in the lighting during the experiment result in a lack of a single reliable I_0 that can be used for each segment, and, consequently, quantitative comparison of rate constants is not justified. It is, however, important to note that the first-order rate constants obtained in

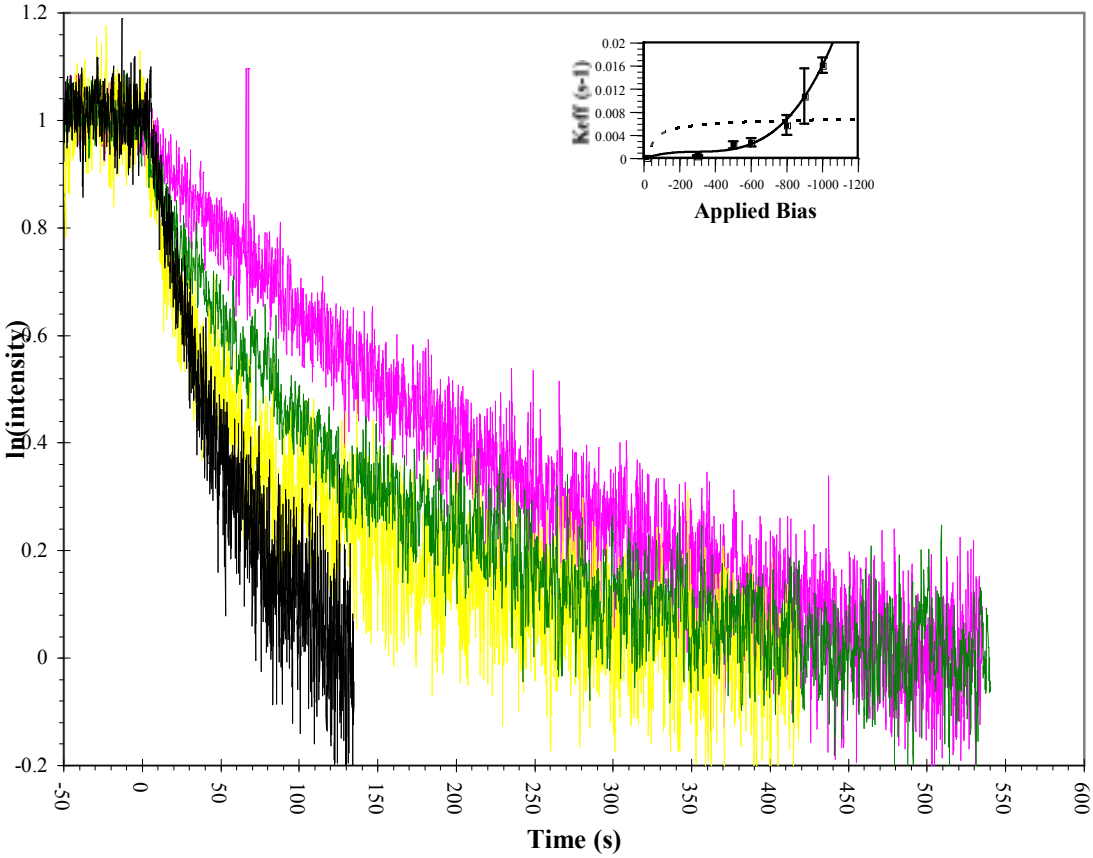

Figure 2.5: RDX exposed to hydrogen plasma at different biases

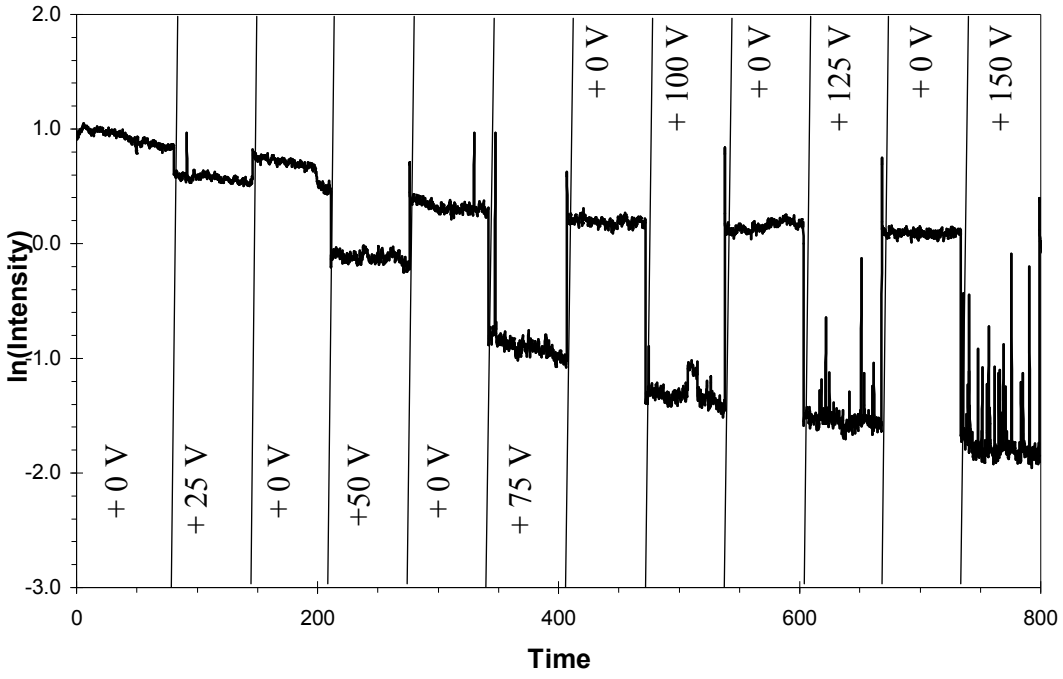

Figure 2.6: The erosion of a RDX film exposed to a hydrogen plasma under an alternating sequence of 0 V applied bias and increasingly positive applied biases

these experiments are consistent with the rate constants measured in all other hydrogen plasmas under 0 V applied bias. No experiments were conducted at higher positive bias due to the building up of charge on small particles within the chamber which resulted in small brilliant explosions that interfere with the video process.

To further address the role of light, a 200 μm thick sapphire wafer was mounted ~2 mm above the surface of the a RDX film. The sapphire window transmits all light between 5 μm and 140 nm, which includes all hydrogen atomic emission lines except the Lyman-α radiation. While transmitting nearly all of the light, the window prohibits charged species, both positive and negative, from impinging on the RDX film, and in addition, placed so close to the surface, the window may also act to reduce the flux of hydrogen atoms arriving at the surface of the film. Figure 2.7 shows the erosion of a RDX film with the sapphire window in place and with the sapphire window removed. For the initial hour shown, the sample was at a floating potential under the sapphire window. Little erosion is observed and an average first-order rate constant of 1.0×10^{-4} s^{-1} is observed. The sample holder was then extracted from the chamber and the sapphire window was removed. Upon reinsertion of the sample (without the sapphire shield), the bias was set at +50 V and the film is observed to erode with an average rate constant of 7.5×10^{-4} s^{-1}, consistent with the low bias rate constant in hydrogen plasmas.

2.D. Discussion

The erosion of RDX films under plasma irradiation is controlled by a number of factors, including chemical composition and applied sample bias. Higher erosion rates are observed in all hydrogen plasmas as compared to argon plasmas. Significant enhancements in the rate of erosion also accompany energetic ion bombardment

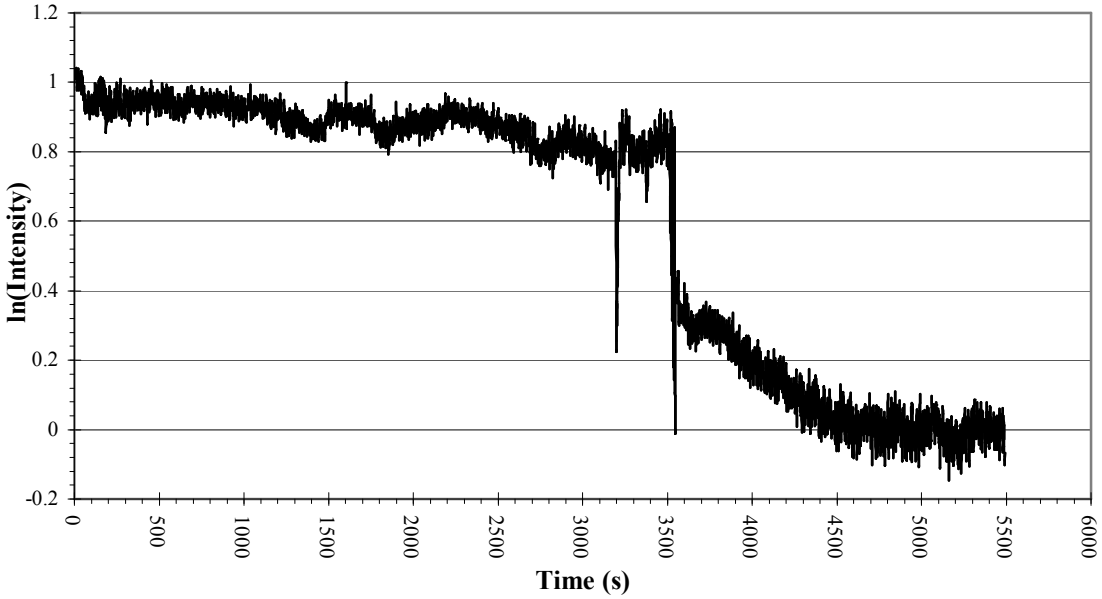

Figure 2.7: Erosion of a RDX film shielded from a hydrogen plasma at +50 V applied bias with a 250 μm thick single crystal sapphire wafer placed above the sample

conditions. No significant enhancements of the rate of erosion are observed due to either electron irradiation or the photon field of the plasma.

Even in chemically inert argon plasmas, where erosion might be assumed to occur by physical sputtering, the experimental data are inconsistent with the predictions of simple physical sputtering theory. This behavior may be inherent to the nontraditional nature of the "sputter target," which is not a typical metallic crystal, but a molecular crystal and a propellant, as well. Propellants, unlike other materials, can combust without any oxygen, which would like lead to additional complex chemical behaviors.

At the microscopic level, physical sputtering can be envisioned, resulting from fast moving ions (atomic or molecular) bombarding a surface. In a matter of a few nanoseconds, the entire energy and momentum of the ion are transferred to the lattice. Traditionally, ion bombardment is expected to result in several outcomes including ejection of surface material (sputtering), implantation of the ions, and roughening of the surface as craters are formed. If the surface being impacted is a propellant, ion stimulated combustion may also be a likely outcome of the bombardment event. The mechanism of ion stimulated propellant combustion can be understood in a number of ways. From an atomistic viewpoint, the glancing angle collision of an ion with a propellant molecule might transfer sufficient energy and momentum to the molecule to initiate combustion. From a continuum viewpoint, the ion bombardment event may be seen as the source of a short-lived, local pressure and temperature spike that may be large enough to initiate the combustion of propellant molecules within a few nanometers of the ion impact point. Either way, the ion impact can initiate combustion. This ion stimulated combustion is the

most reasonable explanation of erosion in argon plasmas at low negative bias and floating potential, where the ion energies are below the threshold for physical sputtering.

Ion bombardment effects are known to vary significantly with ion energy. For instance, very low energy ions, ions with energies below 50 eV, fail to penetrate more than a few layers into a surface and produce little if any physical sputtering. Low energy ions, ion energies between 100 eV and a few thousand eV, penetrate a few nanometers into the surface and result in maximum physical sputtering and surface damage. Medium and high energy ions, with energies of 100 kV and higher, implant hundreds of nanometers into a substrate and produce little damage to the near surface region. It is proposed that the bias induced enhancement observed in these experiments results from a mechanism which is itself an intermediate between the two extremes of energy. At several hundreds of volt negative applied bias, ions may pass through the uppermost layers without interacting significantly with them, only to deposit the bulk of their energy and momentum a few nanometers below the surface. In a propellant, the energy and momentum deposited in the subsurface region may trigger combustion of some propellant molecules. With increasing negative applied bias, the energy and momentum deposited in the local region would increase, and higher extents of combustion would result in a greater release of heat and increased formation of gaseous products. These gaseous products would then be trapped below the surface at high pressure and, for a short period of time, at high temperature. As the surface layers are eroded, even slowly, the subsurface gas "bubbles" could burst through the surface layer and eject additional surface layer molecules from the surface. This is believed to be the mechanism for the

30-fold enhancement of the erosion rate observed in both the argon and hydrogen plasmas under large negative applied bias.

An interesting feature of the proposed energetic ion enhancement mechanism is that it depends on the trapping of subsurface gas, which itself depends on the presence of a dense solid in the near surface region to contain the gas. However, as ion fluence is increased the average damage in the near surface region also increases. At high ion fluence, the near surface region can become highly fractured and even recrystallize or become amorphous. Consequently, at some ion fluence, the near surface region may no longer be able to contain the subsurface gas, causing further energetic ion enhancement to cease, consistent with the observation that the energetic ion enhancement saturates at high ion current, see Figure 2.4.

The minimum rate of erosion of RDX films exposed to hydrogen plasmas is eightfold greater than the equivalent rate in argon. In addition, a similar 30-fold energetic ion bombardment enhancement is also observed in hydrogen plasmas, yielding a maximum rate of erosion in hydrogen plasmas that is also eightfold greater than the highest erosion rates in argon plasmas. The greater rate of erosion observed in hydrogen plasma cannot be attributed to physical effects such as sputtering and, consequently, must be attributed to chemical effect and/or a synergy between chemical and physical effects, such as the energetic ion enhancement mechanism, presented above. Only under a sapphire window, where the access to the surface by reactive species was obstructed, were rates of erosion in a hydrogen plasma equivalent to the lower rates observed in argon plasmas. Although the sapphire window did not transmit the Lyman-α radiation and thus it cannot be completely ruled out as the source of the enhancement in hydrogen

plasmas, it is much more likely that the enhancement is due to the presence of chemically reactive hydrogen atoms. Assuming the hydrogen atoms to be the source of the erosion rate enhancement, a model can be developed that is consistent with all of the hydrogen plasma results. Under all conditions where hydrogen radicals have unimpeded access to the surface, they react with and/or initiate the combustion of RDX molecules that results in a surface erosion rate that is independent of applied bias. Under energetic ion conditions, the hydrogen ions might be implanted a few nanometers below the surface. Upon neutralization they would react with and/or initiate combustion, as they would have on the surface, resulting in trapped gas below the surface. The bursting of the trapped gas through the surface as it eroded down toward the bubbles could result in the ejection of additional molecules in a mechanism similar to the energetic ion enhancement model proposed for argon plasmas. At sufficient simultaneous ion and reactive atom fluence, these "bubbles of reaction" may coalesce and ignite the propellant.

2.E. Conclusion

The electrothermal chemical ignition of propellants has been investigated through experimental modeling. In this method, the complex interaction between the propellant grain and the high-pressure high-temperature gas pulse that emerges from the igniter is probed by exposing thin films of RDX, the model for the propellant, to fluxes of individual components and combinations of those components of the actual ETC pulse, generated with a high-density plasma. By adjusting the applied dc bias on the RDX film sample holder, ions and electrons can be preferentially drawn toward the film with defined energies. Using inert plasmas, the interactions of the RDX film and electrons and generic ions can be investigated in the absence of chemically reactive plasma species.

The erosion rate in argon plasmas was investigated and found to be negligible under electron irradiation. Under ion irradiation, a measurable erosion rate was observed that was found to be consistent with a first-order kinetic process under fixed bias conditions. A 30-fold increase in the erosion rate is observed when the ion energy is increased from −15 V to −800 V applied bias. The enhancement of the erosion rate with increasing ion energy was found to be inconsistent with physical sputtering and has been attributed to the transfer of energy from the ions to the propellant molecules resulting in localized combustion of propellant molecules. In hydrogen plasmas, chemically reactive hydrogen atoms are formed in addition to electrons and ions. Erosion of the RDX films was observed under all bias conditions in hydrogen plasmas. Erosion under electron impact conditions is attributed to chemical processes resulting from the flux of hydrogen atoms at the surface, and represents the minimum erosion rate in hydrogen plasmas. Erosion at zero applied bias and under ion irradiation conditions in hydrogen plasmas was consistently observed to be sevenfold greater than the erosion rate in argon plasmas. Considering the relative mass effects, the hydrogen plasmas may be characterized as being 35 times more effective at eroding the RDX film than the argon plasma. Consequently, the strong synergistic effect between reactive hydrogen atoms and ion irradiation may be attributed to the implantation of hydrogen ions into the solid followed by the reaction of propellant molecules below the surface, yielding “bubbles of reaction” within the solid. At sufficient simultaneous fluence, these bubbles of reaction may coalesce and ignite the propellant.

References

[1]A. Chaboki, S. Zelenak, and B. Isle, IEEE Trans. Magn. **33**, 284 (1997).

2Y Akahoshi, Y. Qu, S. Fukushige, M. Tadaoka, and J. Kitagawa, European Space Agency, [Special Publication] SP, **SP-587**(Proceedings of the 4th European Conference on Space Debris, 2005), 391(2005)

3Y. Akahoshi, E. Matsuda, and H. Hata, From Materials Science Forum, 465 (2004).

[4]H. K. Haak, P. Scaffers, T. H. G. G. Weise, and H. G. Wisken, IEEE Trans. Magn. **39**, 231 (2003).

[5]S. Andreasson and M. U. Carlson, IEEE Trans. Magn. **35**, 181 (1999).

[6]R. A. Beyer and R. A. Pesce-Rodriguez, IEEE Trans. Magn. **39**, 207 (2003).

[7]R. A. Fifer, E. S. Sagan, and R. A. Beyer, IEEE Trans. Magn. **39**, 218 (2003).

[8]M. J. Nusca and M. J. McQuaid, CPIA Publ. **691**, 143 (1999).

[9]M. J. Nusca, M. J. McQuaid, and W. A. Anderson, J. Thermophys. Heat Transfer **16**, 157 (2002).

10V.I. Babushok, , F.C. DeLucia Jr. b, P.J. Dagdigian, J.L. Gottfried , C.A. Munson , M.J.

11Nusca , and A.W. Miziolek, Spectrochimica Acta, Part B: Atomic Spectroscopy, **62B**(12), 1321 (2007)

[12]J. M. Kohel, L. K. Su, N. T. Clemens, and P. L. Varghese, IEEE Trans. Magn. **35**, 201 (1999).

[13]J. Li, T. A. Litzinger, and S. A. Thynell, J. Propul. Power **21**, 44 (2005).

14J. Li, T. A. Litzinger, M. Das, S. T. Thynell, J. Propul. Power, **22**(6), 1353 (2006)

[15]K. Kappen and R. Beyer, Propellants, Explos., Pyrotech. **28**, 32 (2003).

[16]H. F. Winters and J. W. Coburn, J. Appl. Phys. **50**, 3189 (1979).

[17]J. Bardeen and W. H. Brattain, Phys. Rev. **74**, 230 (1948); W. H. Brattain and J. Bardeen, *ibid.* **74**, 231 (1948); W. Shockley and G. L. Pearson, *ibid.* **74**, 232 (1948).

[18]K. Kappen and U. H. Bauder, IEEE Trans. Magn. **35**, 192 (1999).

[19]G.A. Gaddy, S.F. Webb, R. Blumenthal, Plasma Chem and Plasma Processing **19**, 4 (1999).

[20]A. S. Orland and R. Blumenthal, J. Propul. Power **21**, 571 (2005).

[21]Z. L. Zhang, Phys. Rev. B **71**, 026101 (2005).

CHAPTER THREE

EFFECTS ON RDX EROSION RATE WITH MIXED Ar/H_2 PLASMAS

3.A. Introduction

Synergistic effects between simultaneous processes at a surface have been observed in both the plasma etching of silicon[1] and in the erosion of RDX films in pure hydrogen plasmas.[2] In the former case, investigation of the synergistic effect proved critical to the development of a fundamental understanding of the mechanism of plasma etching. To briefly summarize their seminal work on silicon etching, using XeF_2 as a source of F• radicals and an Ar^+ beam as a source of ions, Winters and Coburn[1] observed a synergistic effect between the ions and radicals, in which simultaneous exposure resulted in an etch rate ~8x greater than either acting alone. This strong synergy led to a model of plasma etching where the rate limiting step of etching is the diffusion of radicals through the partially reacted SiF_x layers on the surface and the role of the ions is to thin the partially reacted layer through physical sputtering, dramatically enhancing the diffusion of fluorine radicals to the pristine silicon that lay beneath. This exponential effect on the etch rate is depicted in Figure 3.1. In this work, the erosion rates of RDX films in plasmas fed with mixtures of the hydrogen and argon are determined to elucidate the chemical/physical mechanism underlying the previous observations of strong synergetic effect between ions and radicals observed in the erosion of RDX in pure hydrogen plasmas.

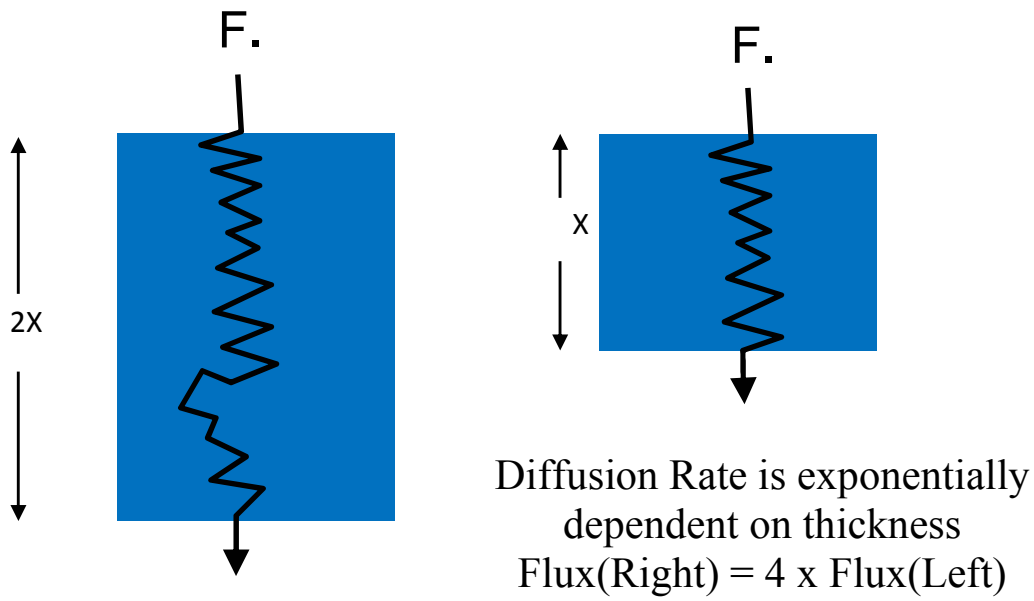

Figure 3.1: A schematic diagram of fluorine diffusion through partially reacted layers of different thicknesses. Due to the exponential thickness dependence of diffusion, doubling the layer thickness reduces the flux by a factor of four.

The synergistic effect between ions and radicals in hydrogen plasmas, observed in previous studies, suggested the possibility that erosion of energetic materials in hydrogen plasmas might take place through a mechanism similar to that observed in semiconductor etching. To test this hypothesis, the erosion rate of RDX films in plasmas of gas mixtures of hydrogen and argon were studied to investigate the effect of introducing an ion of greater mass to a hydrogen plasma. If the mechanism of RDX erosion were similar to that of semiconductor etching, one would expect the addition of argon, with its far more massive ions, to result in enhanced sputtering. This, would in turn result in thinning of any partially reacted layer, which would increase the rate of reactive species diffusion through that layer, ultimately resulting in an increase in the erosion rate of RDX. However, this was not observed. Instead, addition of argon to hydrogen plasmas resulted in reduction of the erosion rate by as much as 40% of the rate without argon in the plasma. This result strongly suggests that the increase in the erosion rate of RDX with increasing sample bias in hydrogen plasmas was not due to an increase in sputtering, but instead, was the result of a chemical reaction mechanism that was enhanced by the increase in sample bias. In light of these results, an entirely new model of the synergistic relationship between the reactive species and the ion energy is proposed where the erosion rate depends on sub-surface hydrogen atom reactions following neutralization of the hydrogen ions with the role of the increased ion energy is to increase the rate and depth of hydrogen ion implantation into the film.

3.B. Experimental

All plasmas were generated with an ASTeX 4300 Compact ECR-Microwave Plasma Source, operated at 200W forward power and a total gas flow rate of

10 SCCM using a MKS model 1159 gas flow regulators and a model 247C controller. An auxiliary magnet, located outside the chamber and ~30 cm downstream of the plasma source, was used to confine the plasma to a cylindrical shape. Concentric rings of RDX were sprayed from 1.0 μg/ml analytic standard solutions in acetonitrile obtained from Cerilliant, as described previously.[3] Each ring was represents ~0.1 ml of solution or a total of 0.1 mg of RDX.

Video images of the erosion films of RDX were recorded on videotape using a commercial surveillance camera from which the infrared illumination diodes had been removed. In most experiments, the films were illuminated with elliptical spot, E.O. Edmund Model Y52-094 (5.0mW @ 670 nm) diode laser at a glancing incidence, with an E.O. Edmund Model Y43-087 narrow bandpass interference filter (671 nm) in front of the camera lens to maximize the ratio of laser light scattered from the deposited film to light from the plasma. The -500V dc-bias was maintained on the substrate by a KEPCO BOP 1000M bipolar operation amplifier.

Kinetic analysis was also carried out as described previously in Chapter 2. Briefly, first-order kinetics was applied directly to the scattered intensities under the assumption that the scattered light intensity was proportional to the amount of RDX remaining on the substrate. These simple relationships have proven adequate in the previously work, and are consistent with current data.

3.C. Results

If the erosion of RDX were to behave like semiconductor etching, the introduction of a much more massive ion, like argon (m/z = 40), to a hydrogen plasma that consists of the ions, H^+ (m/z = 1) and H_2^+ (m/z = 2), would significantly increase the

erosion rate by thinning the partially reacted layer and allowing for the diffusion of the reactive species from the plasma to the pristine material below the surface layer. Experiments were conducted to test the validity of this idea in mixed hydrogen-argon plasmas with a total gas flow of 10 SCCM varying the amounts of hydrogen and argon. Rate coefficients are plotted against percent hydrogen in Figure 3.2 to display how the erosion rate of RDX is affected when adding argon to a pure hydrogen plasma.

Upon substitution of argon for hydrogen plasmas, the rate of erosion decreases, implying the synergy between ions and radicals that occurs in semiconductors is not observed in energetic materials. In fact, the argon seems to act as a quenching agent in mixed hydrogen-argon plasmas. As more and more argon is added, the erosion rate drops with the minimum being at 40% argon. After substitution of greater than 40% argon, there is an increase in the erosion rate, but it fails to exceed that of a pure hydrogen plasma. The erosion rate of RDX is greatest in a pure hydrogen plasma as opposed to a hydrogen-argon mixture.

3.D. Discussion

One possible explanation for the lack of an increase to the erosion rate upon substitution of argon for hydrogen in mixed hydrogen-argon plasmas is that the argon does not become ionized. If the argon does not become ionized in the plasma, then it would not be drawn to the surface of RDX by a negative bias and no significant thinning of the layers will occur. To examine the likelihood of this explanation, ratios of H^+ ions to Ar^+ ions and H_2^+ ions to Ar^+ ions were determined via a Boltzmann probability of ionization,

$$N_b/N_a = (g_b/g_a)(e^{-(Eb-Ea)/kT}), \quad (3.1)$$

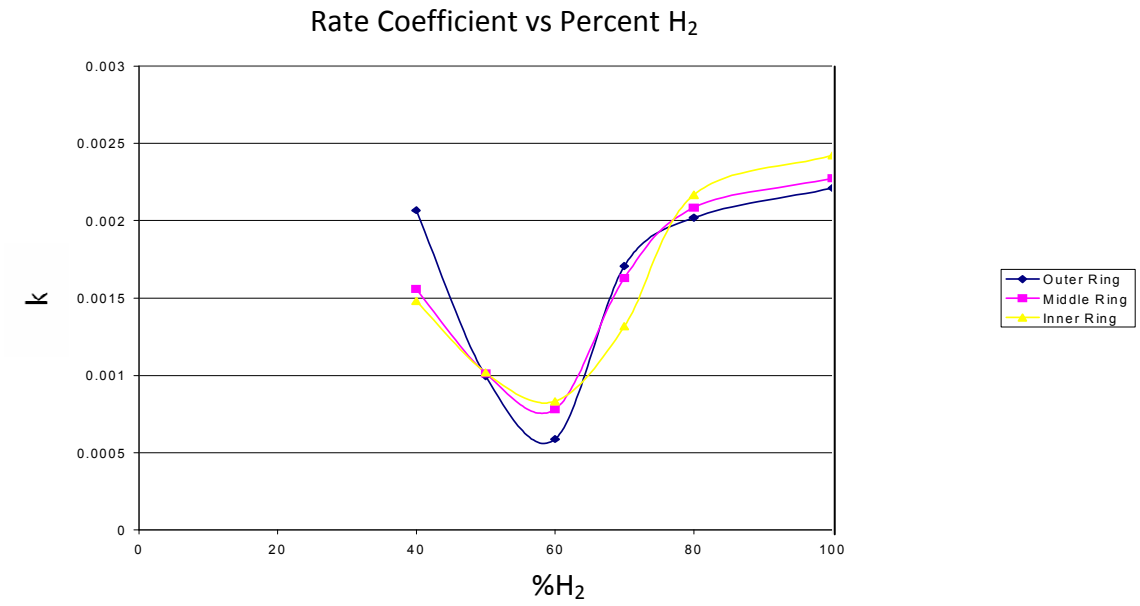

Figure 3.2: Rate Coefficient vs Percent Hydrogen

where a and b are the respective ions, N is the number of ions, g is the degeneracy, E is the first ionization energy, k is the Boltzmann constant, and T is the electron temperature. The ionization potentials for argon, hydrogen molecules, and hydrogen atoms are 15.76, 15.43, and 13.60 eV,[4] respectively. Electron temperatures found in ECR microwave plasmas range between 2000-12000 K.[5] Calculations were done over this range, see Figures 3.3 and 3.4, show that in the range of temperatures found in ECR microwave plasmas, the hydrogen ions are prevalent in both cases. A temperature of 6000 K was chosen arbitrarily because it falls in the middle of the range of temperatures found in ECR plasmas. At 6000 K, it can be seen that there is one Ar^+ ion for every two H_2^+ ions. The H^+:Ar^+ ratio shows that at 6000 K, approximately 1.5% of the argon is ionized. Dependent on the square root of the masses, Ar^+ sputters 6.3 times faster than H^+. The rate of sputter of Ar^+ was calculated from -600 V and 1.76 mA to be approximately 7000 Å/s. 1.5% of the argon ionized gives a sputter rate of ~ 100 Å/s, which should effectively thin a ~ 30 Å reacted layer. Since there is still a significant amount of charge on the argon, this discredits the argument that ionization on the argon does not occur.

Therefore, a new mechanism is required to account for the hydrogen attack of the propellant films. An ETC ignition model is proposed where hydrogen ions from the high density, high pressure plasma implant into an RDX crystal. The ions are then neutralized, to produce hydrogen atoms that attack RDX resulting in the formation of gases and release heat resulting in sub-surface bubbles of hot, highly pressurized gases. These "hot spots" grow and coalesce into a detonation front. This is depicted in Figure 3.5.

The first step in our mechanism is the neutralization of H+ ions by RDX, where calculations were carried out.[6] Then, one might suspect that the hydrogen atom attack

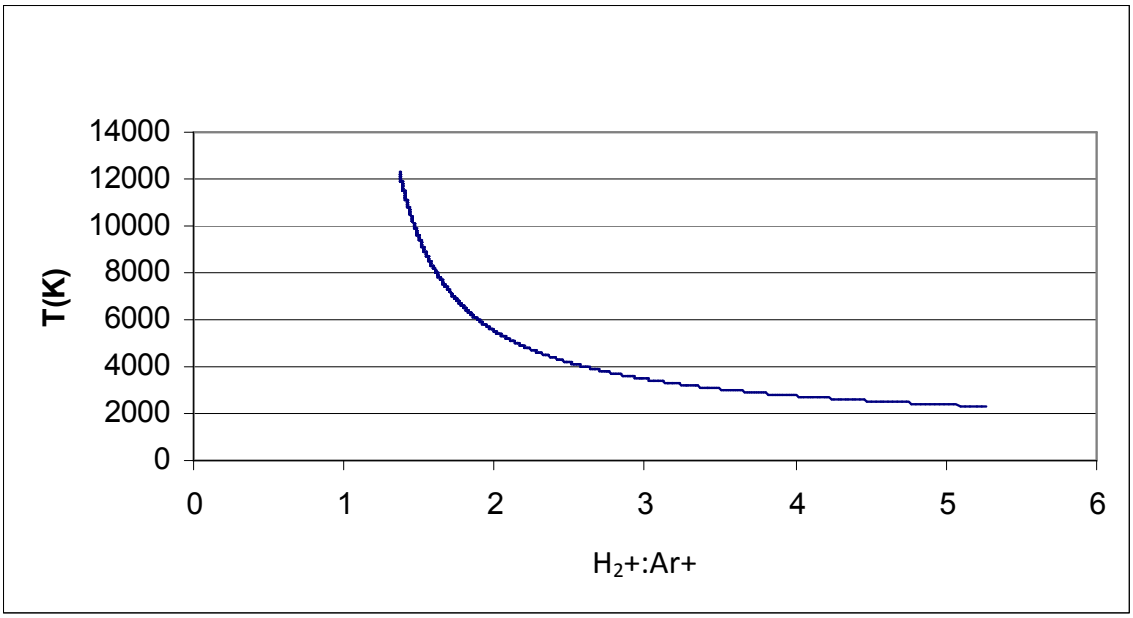

Figure 3.3: H_2^+:Ar^+ at temperatures found in ECR plasmas. At 6000 K, there is ~ one Ar^+ for every two H_2^+.

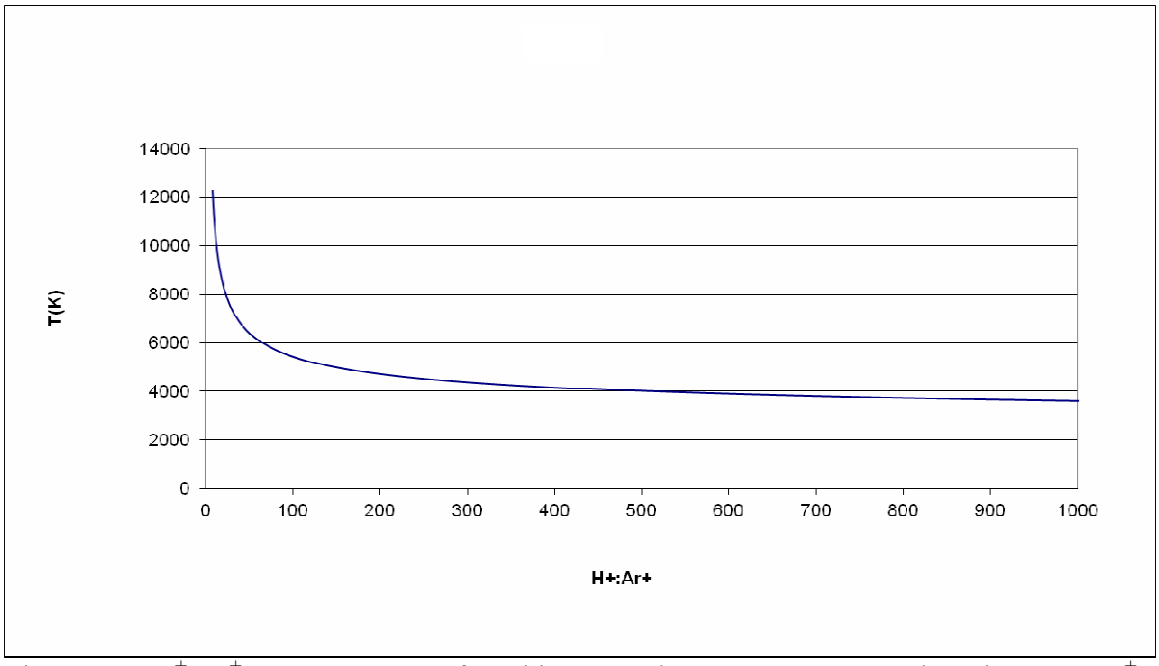

Figure 3.4: H^+:Ar^+ at temperatures found in ECR plasmas. At 6000 K, there is ~ one Ar^+ for every seventy H^+.

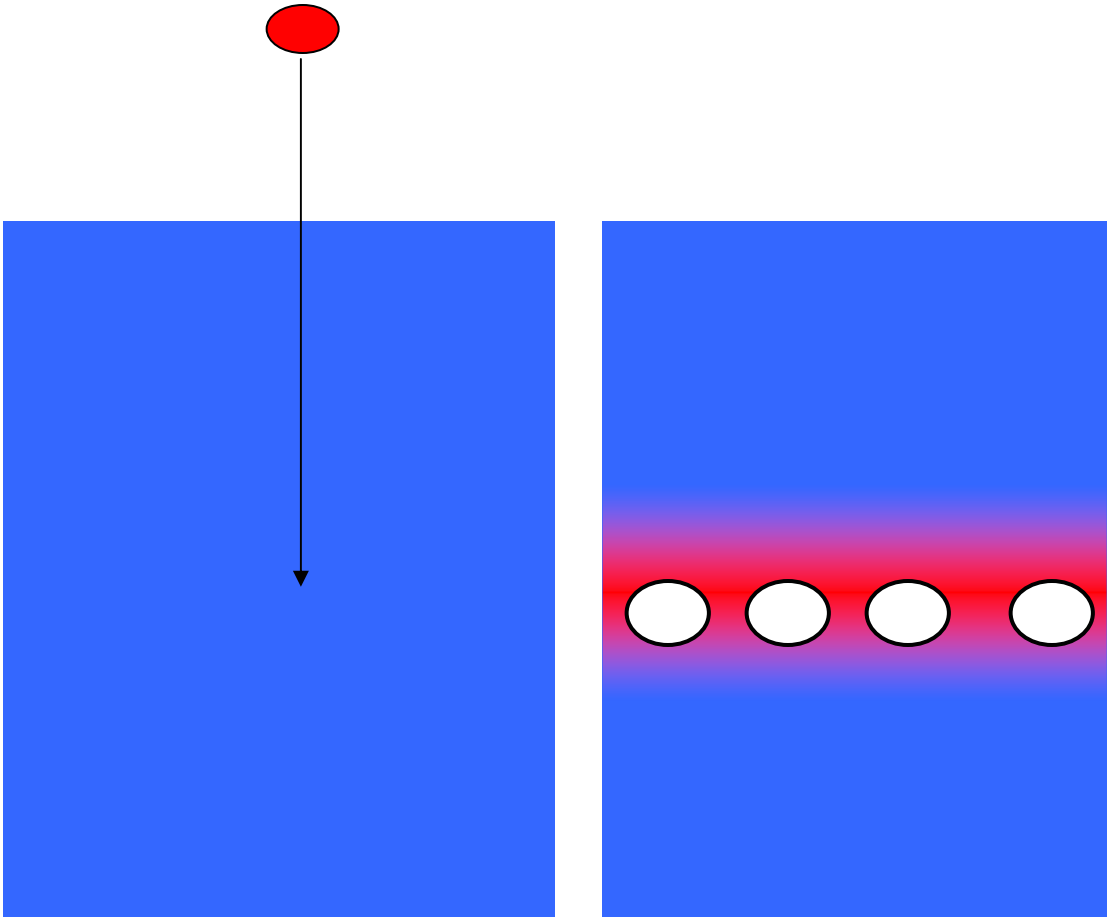

Figure 3.5: Scheme of H implantation into RDX results in subsurface formation of hot dense gas that under sufficient ion flux may coalesce into a detonation front.

might follow the Goddard mechanism of thermal decomposition where the NO_2 group attacks the hydrogen atoms on the backbone of the RDX ring resulting in the HONO intermediate.[7] This is depicted in Figure 3.6. The Goddard model has been investigated theoretically and found to have an enthalpy of reaction of 24 kcal/mole, making it slightly endothermic. The enthalpy of reaction was calculated by:

$$\Delta H_{reaction} = \Sigma \Delta H_{products} - \Sigma \Delta H_{reactants} \quad (3.2)$$

This mechanism is debatable, however, because not only is this mechanism is endothermic, but because of the increased degrees of freedom, it is slightly exergonic. However, further reaction of the HONO and HCN creates 3 N_2, 3 CO_2 and 3 H_2O, which is highly exothermic.

Hydrogen atoms can attack the RDX via two paths. Similar to the Goddard model, one path, as depicted in Figure 3.7, shows the hydrogen atom attacking the NO_2 group, resulting in the release of a HONO and leaving a radical on the nitrogen of the RDX ring. Although this mechanism is exothermic, there is a good possibility that when the radical formed on the nitrogen of the RDX rings comes in close proximity to HONO intermediate subsurface, that the reverse reaction will occur. Conversely, another model, suggested by previous observations from CVD deposition of diamond films from primarily hydrogen plasmas involves the abstraction of hydrogen from carbon in the RDX ring. This is similar to the chemistry found in the chemical vapor deposition (CVD) for diamond growth where hydrogen is stripped from the backbone of the hydrocarbon.[8] The new mechanism is shown in Figure 3.8 The first step is the hydrogen abstraction. In the second step, the electron left from the hydrogen abstraction, on the carbon, combines with an electron from the nitrogen-nitrogen bond. This forms a double bond between the

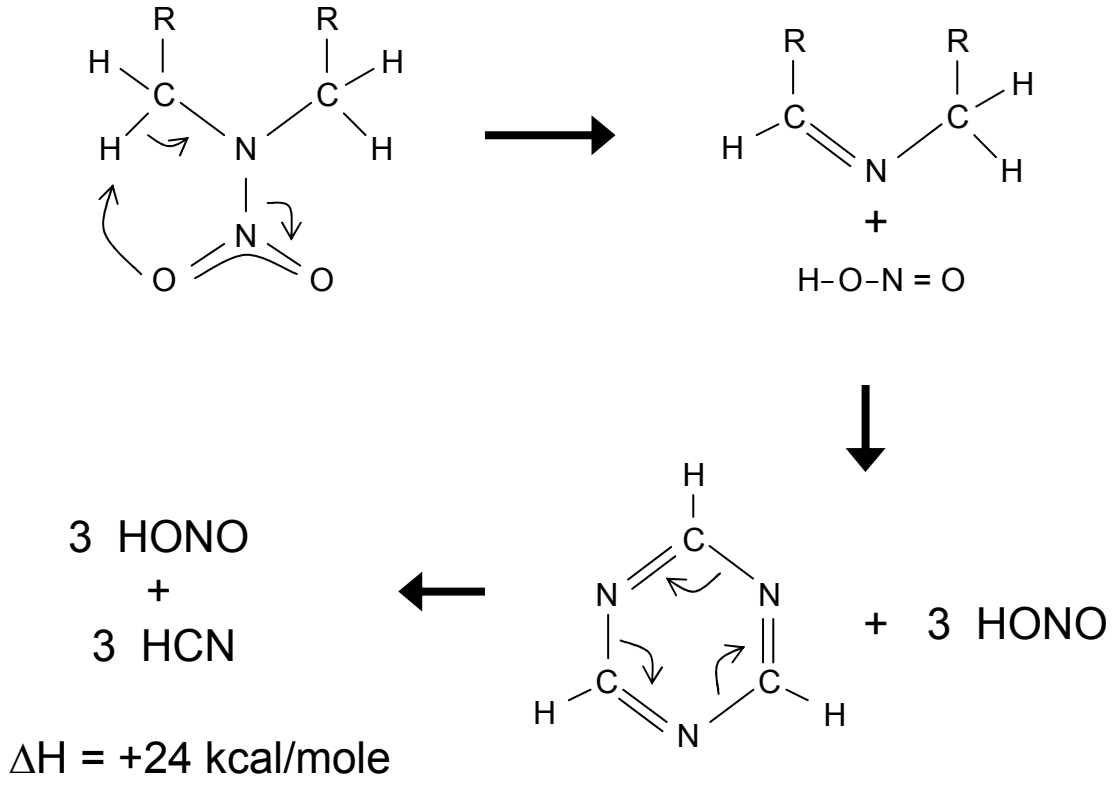

Figure 3.6: Goddard Model for the Thermal Decomposition of RDX

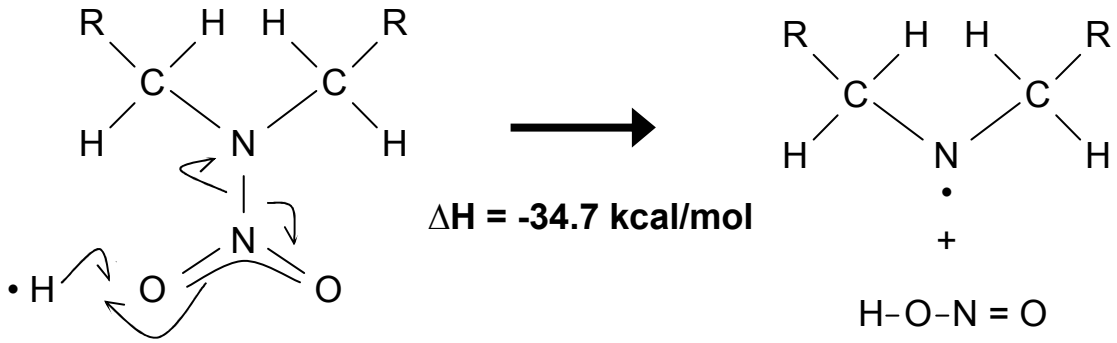

Figure 3.7: Hydrogen attacking the RDX ring via the NO_2 group

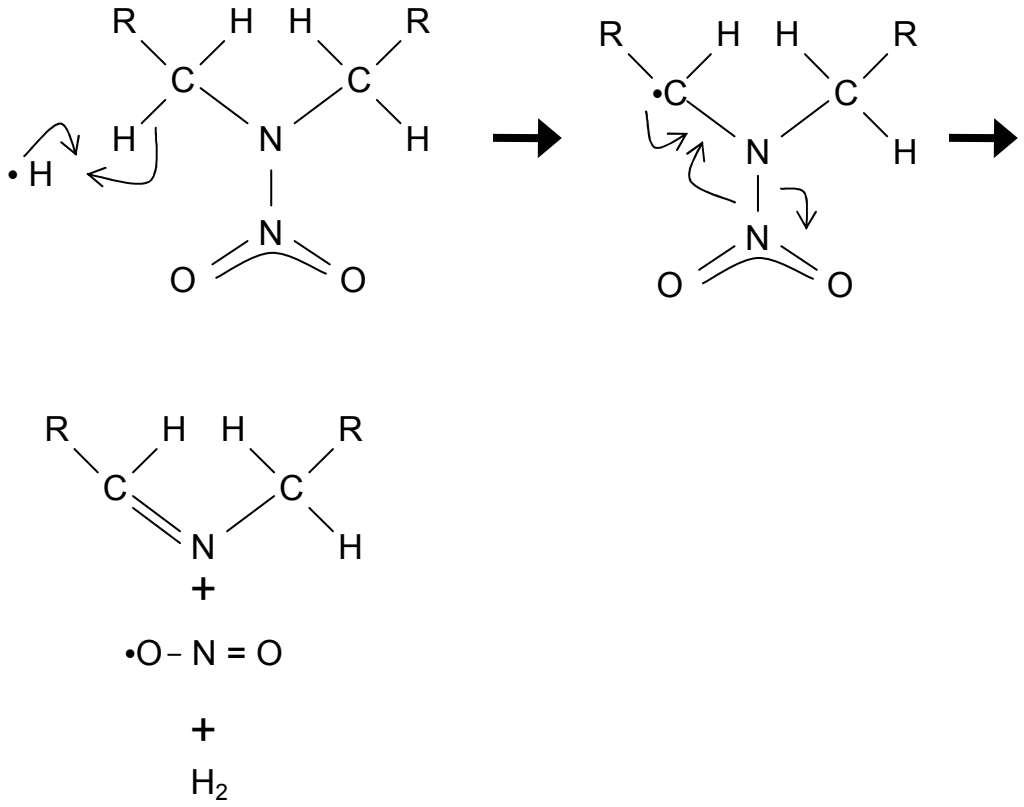

Figure 3.8: Proposed stepwise mechanism of H abstraction from the RDX ring

carbon and nitrogen and allows for nitro group to the leave the ring as products along with the hydrogen molecule. All three of these species are stable and a reverse reaction is very unlikely to occur. The enthalpy of reaction was theoretically determined to be -28.5 kcal/mole, making it exothermic.[6] Also, since this mechanism leads to the formation of H_2 and NO_2, these gases are then trapped, and the heat released below the surface converts the mechanism from that of a secondary explosive to that of a primary explosive.

3.E. Conclusion

Experiments were performed to investigate whether adding argon to a hydrogen plasma would greatly enhance the erosion rate of RDX films. It was found that the greatest erosion rate occurred in a pure hydrogen plasma. Therefore, a new mechanism was introduced where hydrogen is abstracted from the RDX ring. It can be shown stepwise as follows:

$$H^+_{(plasma)} + RDX_{(soild)} \rightarrow H^+_{(subsurface)}$$

$$H^+_{(subsurface)} + RDX_{(solid)} \rightarrow H\cdot + RDX^+_{(solid)}$$

$$RDX^+_{(solid)} + RDX_{(solid)} \rightarrow RDX_{(solid)} + RDX^+_{(solid)}$$

$$H\cdot + RDX_{(solid)} \rightarrow H_{2(g,\ subsurface)} + NO_{2(g,\ subsurface)} + C_3H_5N_5O_4 + Heat$$

$$H_{2(g,\ subsurface)} + NO_{2(g,\ subsurface)} \rightarrow H_2O_{(g,\ subsurface)} + NO_{(g,\ subsurface)} + Heat$$

$$Heat + Pressure \rightarrow Spontaneous\ Combustion.$$

References

[1]R. Valliere and R. Blumenthal, J. Appl. Phys. **100**, 084904 (2006).

[2]J.W. Coburn and H. F. Winters, J. Appl. Phys. **50**, 3189(1979).

[3]A.S. Orland and R. Blumenthal, J. Prop. Power, **21(3)**, 571 (2005).

[4]NIST Chemistry WebBook, WWW document, (http://webbook.nist.gov/chemistry/)

[5]I. Brown, in *Handbook of Ion Sources*, edited by B. Wolf, (CRC Press, Inc., Salem, 1995), 18.

[6]M. McKee, (Private Communication).

[7]A. Strachan, E.M. Kober, Adri C.T. van Duin, J. Oxgaard, and W.A. Goddard, J. Chem. Phys. **122**, 054502 (2005).

[8]P.W. May, Endeavour Magazine, **19(3)**, (1995).

CHAPTER FOUR

DESIGNING A CARBON FLUX APPARATUS

4.A. Introduction

Carbon atom sources have been needed throughout the scientific community for a variety of reasons. Most notably, they have been implemented in the generation of C-60 (buckminsterfullerene)[1] and nanotubes.[2]

Earlier, in Chapter 2, ETC ignition was described where a polyethylene tube replaced lead azide, or black powder, which were found in conventional ignition of large bore artillery. This polyethylene tube was attached to a large capacitor, and when discharged, temperatures reaching 30,000 K were achieved. At temperatures above 10,000 K, the chemical bonds in molecules dissociate into individual atoms and ions, forming a dense plasma. Therefore, the species that can be found in a plasma generated from polyethylene are light[3], electrons, hydrogen atoms, hydrogen ions, carbon atoms, and carbon ions.[4] The individual and synergistic roles of light, electrons, hydrogen atoms, and hydrogen ions with RDX were described in great detail in Chapter 2. A source of carbon atoms and ions needed to be generated to understand their respective roles on the erosion rate of RDX. A picture of how the device would be implemented into the ECR-Microwave plasma that was described in Chapter 2 is depicted in Figure 4.1.

4.B. Original Design

Inspired by a devices created by Shevlin[5] and Skell[6], an apparatus was designed to provide a carbon atom flux into the plasma chamber for the purpose of studying the erosion of RDX films. Figure 4.2 depicts a sketch of the first generation device that was a

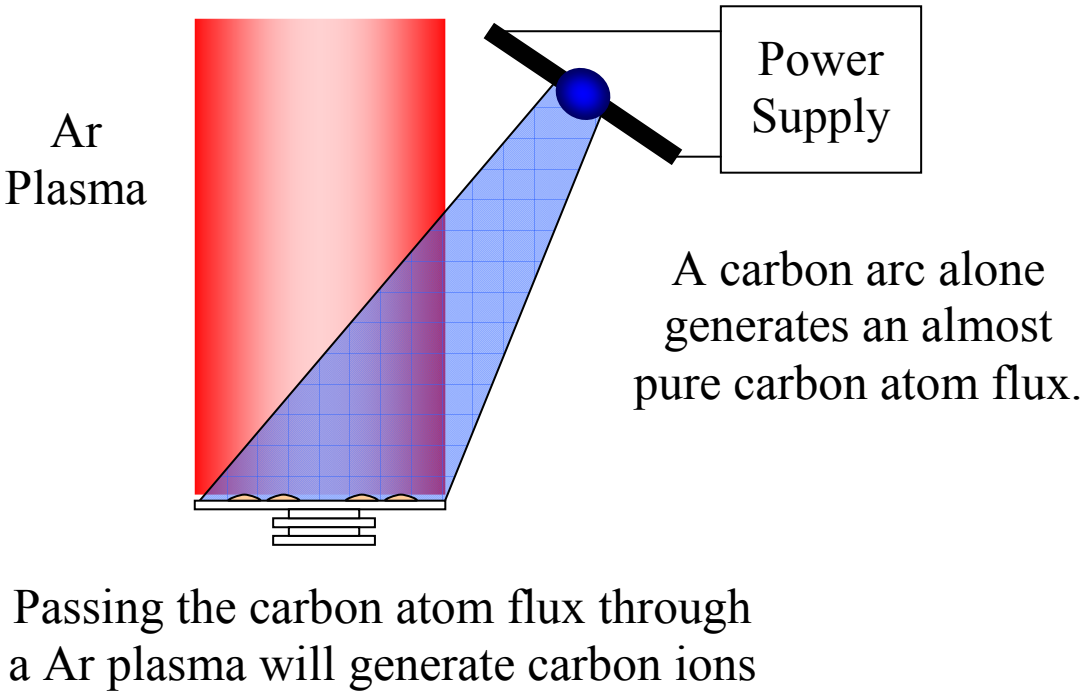

Figure 4.1: Generating carbon atoms and ions

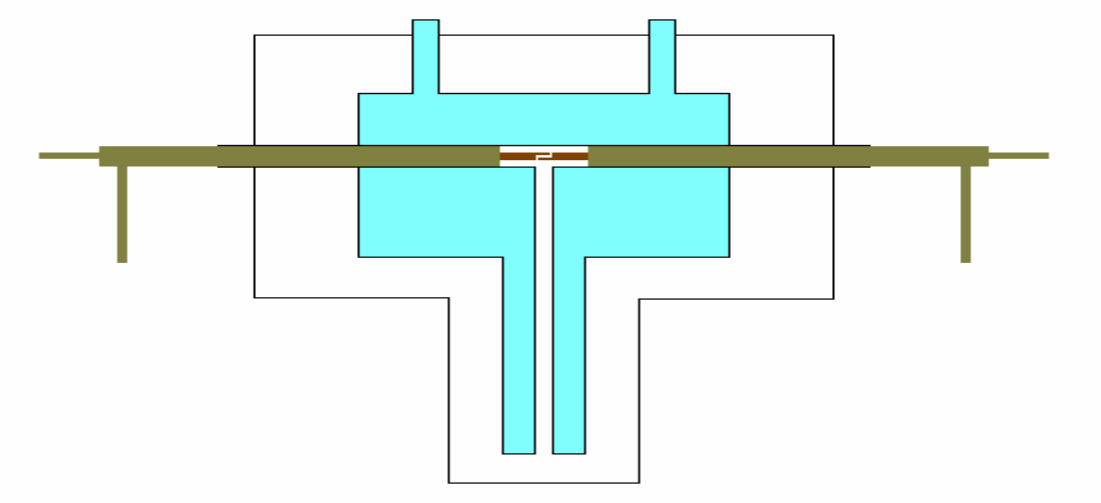

Figure 4.2: Sketch of First Generation Carbon Flux Apparatus

vacuum vessel constructed out of glass in a basic "T" design. Water-cooled brass electrodes entered the chamber through the horizontal arms using o-ring seals to allow for control the insertion distance and to maintain vacuum. In addition, there was an o-ring seal at the bottom of the apparatus that went to vacuum. Inserted into the electrodes were graphite rods placed into contact with one another. As a power source, hose clamps were used to attach the leads of an arc welder. When turned on, the welder produced a pure carbon arc between the two graphite rods. Carbon atoms were allowed to freely travel down the tube at the bottom to be collected on a glass slide. All other atoms were collected on the surface of the liquid nitrogen super-cooled glass. In theory, this design allowed for a 3.81 cm carbon disc to be produced on a sample positioned 29.5275 cm below the arc at a 40° angle from the horizontal.

Early tests of the original carbon atom apparatus showed that no arc would be produced unless the rods were initially placed in direct contact with one another and that no arc would be maintained if the rods were not kept close together. Another drawback of the initial design was that the outer jacket had a tendency to frost over due to the thermal conductivity of pyrex as the liquid nitrogen cooled the outer layer of glass. The first version of the carbon apparatus ultimately suffered catastrophic failure when gases created from the carbon arc collected at the top of the t-connection and allowed heat to rise and melt a large portion of the pyrex. Being under vacuum, the softened glass was drawn inward until a large hole was produced that broke vacuum and allowed liquid nitrogen to wash over the electrodes.

4.C. Modified Design

The second design of the carbon apparatus took into account many of the shortcomings of the first device. Figure 4.3 above shows many of the differences between the two designs. To prevent the gas collection that allowed heat transfer which caused structural failure to the first apparatus, the second device was fitted with a pump port to allow gases that were not successfully removed through the 0.9525 cm tube in the bottom to be pulled from the system. A second improvement over the prototype was doubling the distance between the liquid nitrogen compartment and the outer jacket of the device. By increasing this distance from 1.0 cm to 2.0 cm, the frosting effect that plagued early tests was eliminated. The second apparatus was also made smaller to cut down on the amount of time necessary to fill and empty the liquid nitrogen region.

Ultimately the second carbon atom apparatus suffered critical failure as well. A small soft spot developed under the location of the arc and was drawn inward by vacuum until a hole developed that allowed liquid nitrogen to supercool the graphite rods and prevent an arc from occurring.

In the only experiment to produce quantifiable results, running the second carbon atom apparatus for thirty minutes with 4.0 volts pushing 90.0 amps through the system produced 0.0099g of sample that was collected on a 1.27 cm by 1.27 cm glass slide. Early attempts to test this sample have yet to provide results. Future designs of the carbon apparatus are currently being considered. Among the possible changes is the changing of the t-connection within the device from pyrex to quartz. It is believed that the latest of the two structural failures was due to local deposition of carbon on the glassware. This local deposit would have had a much higher temperature than the surface of the glass and would also be black in color. This black colored deposit would not allow light to pass

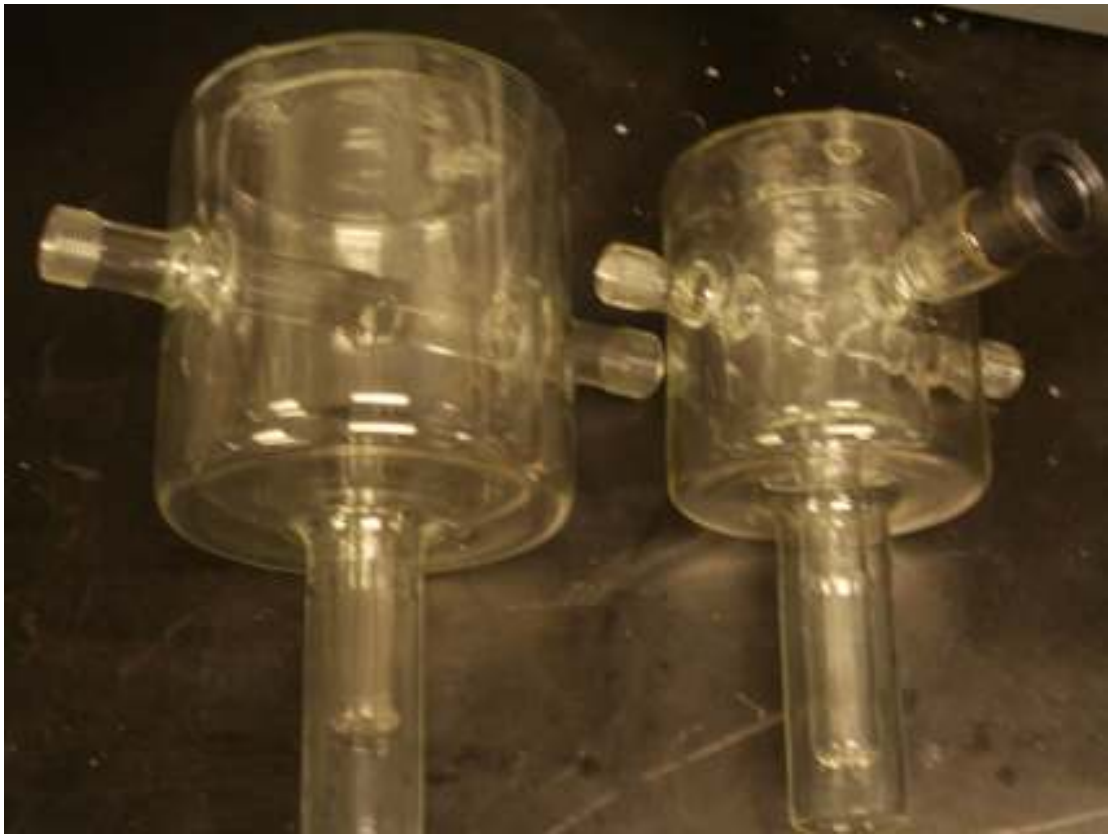

Figure 4.3: First and Second Generation Carbon Flux Apparatus

through as easily and would therefore absorb more radiant energy from the carbon arc, thereby raising the temperature locally far above the 1089K needed to soften pyrex.

It is believed that the melting of the pyrex occurred due to local carbon deposition rather than part of a general melting trend along the entire surface of the glassware because the thermal conductivity of pyrex prevents the surface of the glassware from achieving a temperature above 250 K when the applied power is 360 watts. This 250 K is not enough to have any structural effect on pyrex. The following equations help illustrate this:

$$dQ/dt = -KA\,(dT/dx), \tag{4.1}$$

$$\text{Power} = (1.005\ \text{W/mK})(20.6\text{x}10^{-4}\ \text{m}^2)(1012\ \text{K}/1\text{x}10^{-3}\ \text{m}) = 2.095\ \text{kW}, \tag{4.2}$$

K is the thermal conductivity of pyrex from literature values[7], A is the measured surface area of the device, dT is the calculated difference between the softening pt of Pyrex (1089K) and liquid nitrogen (77K), and dx is the thickness of the Pyrex .

$$\text{Power} = KA\,(T_f\text{-}T_i/\text{thickness}) \tag{4.3}$$

$$360\ \text{Watts} = (1.005\ \text{W/mK})(20.6\text{x}10^{-4}\ \text{m}^2)[(x\text{-}77\text{K})/1\text{x}10^{-3}\ \text{m}],\ x = 250\ \text{K} \tag{4.4}$$

$250\ \text{K} << 1089\ \text{K}$

Another design change that will be implemented in future designs is that the diameter of the t-connection will be widened to increase the surface area of the inner wall to give a larger area for heat to transfer and also to try to further scatter the particles that could deposit on the glassware.

References

[1]D. M. Cox, K. C. Reichmann, and A. Kaldor, J. Chem. Phys. **88**, 1588 (1998).

[2]M. Yudasaka, R. Kikuchi, T. Matsui, Y. Ohki, S. Yushimura, and E. Ota, Appl. Phys. Lett. **67**, 2477 (1995)

[3]K. Kappen and U. H. Bauder, IEEE Trans. Magn. **35**, 192 (1999).

[4]M. J. Nusca, M. J. McQuaid, and W. A. Anderson, J. Thermophys. Heat Transfer **16**, 157 (2002).

[5]P. B. Shevlin, "The Preparation and Reaction of Atomic Carbon". In R. A. Abramovitch. *Reactive Intermediates,* New York: Plenum Press, **1**, 1 (1980).

[6]P. S. Skell, J. J. Havel, M. J. McGlinchey, Acc. Chem. Res. **6**, 97 (1973)

[7]The Engineering Tool Box, WWW document, http://www.engineeringtoolbox.com/thermal-conductivity-d_429.html.

CHAPTER FIVE

CONTROLLING RDX PARTICLE SIZE VIA A NEBULIZING SPRAY TECHNIQUE

5.A. Introduction

Siviour et al studied the sensitivity of explosives with two RDX/HTPB polymer bonded explosives, with different explosive particle size, using a Hopkinson bar system at three different temperatures.[1] Studying the mechanical properties, it was found that the strength of the material decreases with increasing particle size. Increasing the temperature of the material also decreases its strength, but not the nature of its response to detonation. The temperature effect on sensitivity of larger particle size materials is smaller, which is expected because the larger particle size material is governed to a greater extent in its mechanical properties by the relatively temperature insensitive explosive crystals[1]. This may be true for polymer bonded explosives, but for pure crystalline propellants, the results seem to differ. For example, pure HMX on the centimeter-scale can be impacted with a flyer-plate at a velocity known to ignite composite powders and nothing happens, showing that it is greatly insensitive[2]. It is believed in the field that composite powders with two different size particles (displaying a 10:1 size ratio) are vital to ignition. A flyer-plate hits the propellant causing a shockwave to compress the composite powder. This then causes the particles' jagged corners to rub against each other and create friction. This friction leads to hot spot formation, which starts ignition. Among the many models for the ignition, this is known as the intercrystalline model, which happens to be the most popular explanation for RDX detonation.

The formation of hotspots depends upon the energy input and the physical properties of the explosive composition. The diameter of the hotspots is in the region of 0.1-10 μm and their duration is about 10^{-5}-10^{-3} seconds with temperatures greater than 900ºC.[3]

The energy from the stimulus is converted into heat by adiabatic compression of small, entrapped bubbles of gas. When gases are compressed, heat is generated, or more accurately, energy is transferred. If the rate of heat generation within a system exceeds the rate of heat loss (energy transfer) to the surroundings, the temperature of the system will rise. If the rate of compression is rapid enough such that the heat loss may be considered negligible, resulting in "adiabatic compression", the temperature rise will depend on compression ratio.[4] The heat generated forms hotspots. For an ideal gas, the temperature inside the gas bubbles T_f depends on the compression ratio as shown in the equations,

$$T_f = T_i(P_f/P_i)^{(\gamma-1/\gamma)} \text{ and} \quad (5.1)$$

$$P_f = P_i(V_i/V_f)^{\gamma} \quad (5.2)$$

where T_i is the initial temperature of the bubble, P_i and P_f are the initial and final pressures inside the bubble respectively, V_i and V_f are the initial and final volumes of the bubble, and γ is the ration of the specific heats. From equation 5.1, it can therefore be seen that when the initial pressure of the gas is raised, the temperature inside the bubble is increased as well. The minimum temperature rise in the gas bubble is assumed to be about 450ºC for ignition to occur. This effect can be observed in the performance of a liquid when subjected to impact at different pressures. When liquid nitroglycerine is

subjected to an impact energy of 5000g/cm at an initial pressure of 1 atm an explosion occurs. If the initial pressure is raised to 20-30atm, however, no explosion is observed.[3] The minimum volume is fixed by the incompressible liquid air in the void. As the initial pressure increases, the initial amount of substance increases. Therefore, the final volume increases and consequently, V_i/V_f, decreases.

"Under certain conditions, these microscopic bubbles can result in an extremely sensitive explosive which can then be ignited by the gentlest of blows. If precautions are taken to eliminate all the bubbles, the explosive becomes comparatively insensitive, and very high impact energies must be used for ignition. Under these conditions, the ignition is due to the viscous heating of the rapid-flowing explosive as it escapes from between the impacting surfaces.

Another source of hotspots is the presence of grit particles, such as crystals. When the particles are small and sharp, only a small amount of friction or impact energy is needed to produce a hotspot. This is because localized energy is generated at the stress points; soft particles are unable to generate enough energy to produce hotspots since they will be crushed or squashed. Some explosive compositions which contain a polymer as a binder can also be quite sensitive to impact; this is due to the polymer failing catastrophically and releasing sufficient energy to form hotspots.

Ignition, therefore, begins at a hotspot, but does not always lead to detonation. If the energy lost to the surroundings is greater than the energy generated by the hotspots, the small micro-explosions die away without further propagation. If a particle of an explosive is smaller than a certain minimum size (which may be called 'critical'), the dissipation of heat will be greater than its evolution and no explosion will take place."[3]

Primary explosives will ignite below the melting point of the crystals where as secondary explosives will ignite above the melting point.[3] When solid explosives are subjected to high impact, hotspots are formed from compression and heating of the trapped gases, and from friction between crystal particles. Ignition for the majority of primary explosives is via hotspots generated by intercrystalline friction, whereas ignition in secondary explosives is from hotspots generated through the compression of small gas spaces between the crystals.[3] The difference between the formation of hotspots in primary and secondary explosives is related to the melting points of the crystals.

"When a secondary explosive is subjected to high impact, the material will flow (called 'plastic flow') like a liquid entrapping small gas bubbles. Hotspots will be generated by the compression and heating of the trapped gases similar to the process described for the formation of hotspots in liquid explosives, except that the impact energies needed for ignition will be far higher. Hotspots which are generated by impact are transient and will only last for a very short time in the order of microseconds. Consequently, hotspot temperatures for ignition are higher than conventional thermal ignition temperatures for explosive substances."[3]

To better understand the structure of films deposited by a nebulizing spray technique, powder x-ray diffraction was performed and RDX particle size was determined. The nebulizer can achieve the optimal ratio (10:1),[2] which is vital for ignition, for particle size simply by depositing a film of certain size and manipulating a few variables, depositing a film that is ten times larger or smaller.

5.B. RDX Crystal Data

RDX crystallizes in the orthorhombic space group, Pbca, where a = 13.182 Å, b = 11.574 Å, and c = 10.709 Å. The Miller indices were assigned with corresponding 2θ angles in Figure 6.1.

5.C. Experimental

A diagram of the nebulizing spray set up is displayed and described in Chapter 2. The RDX sample, dissolved in acetonitrile, was fed through a capillary with a syringe pump. The fast-moving, dry, sheath gas (N_2), desiccated the droplets that emerge from the capillary and carried them along to deposit on the glass substrate, where a thin film of RDX remained.

A number of variables were studied when using the nebulizing spray technique, as described previously, in determining what factors contribute to the distribution of particle sizes. The factors that were studied are concentration, flow rate, gas flow, and spraying distance. The concentration was changed by dissolving different amounts of RDX powder into a given amount of acetonitrile. The flow rate was varied using a syringe pump that would push the RDX solution through the capillary in mL/hr. The gas flow was controlled using a pressure gauge on the house nitrogen, which was boil-off from the building's liquid nitrogen tank, used for the carrier gas. Spraying distance is the distance from the nozzle to the glass substrate. An ideal range was determined through experimentation that the sprayer was close enough to the glass substrate that the RDX

(h,k,l)	2θ
1,1,1	13.218
1,2,0	15.498
0,0,2	16.499
1,2,1	17.698
2,2,0	20.408
0,2,2	21.350
2,2,1	22.096
1,2,2	22.733
2,1,2	23.569
3,1,1	25.355
0,3,2	26.196
0,4,0	26.992
1,4,0	28.502
1,2,3	29.459
2,3,2	30.485
2,4,0	31.133
2,2,3	32.410
1,3,3	33.286
0,1,4	34.052
4,0,2	35.158
1,5,1	35.882
1,2,4	36.971
4,3,1	38.109
2,2,4	39.480

Figure 5.1: Table of Miller indices and corresponding 2θ angle for RDX

particles would hit the substrate, but far enough away that the accumulated liquid solvent does not float away the smaller crystallites and clustering into large crystals, forming a circle devoid of RDX as opposed to a uniform, ring-shaped film.

X-ray Diffraction was performed using a Bruker D8 Discovery with GADDS. The GADDS is the large area detector. The samples were scanned over 90 degrees and spectra were obtained.

5.D. Results

Powder x-ray diffraction was performed on a series of RDX films and spectra were obtained. Figure 5.2 depicts an example of the raw data. From this raw data, a Gaussian fit was performed on each peak corresponding to each Miller index. The FWHM was calculated and a weighted diameter was determined from using the Scherrer equation,

$$\tau = K\lambda/\beta\cos\theta, \qquad (5.3)$$

where τ is particle size, K is the shape factor, λ is the x-ray wavelength, β is the FWHM, and θ is the Bragg angle. The shape factor is a dimensionless quantity that typically has a value of .9 for Gaussian fits. The weighted diameters of the RDX particles were determined to range from 3.1 to 7.4 nm depending on experimental conditions.

Single component analysis was performed to establish any linear relationships between the variables: concentration, flow rate, gas flow, and spraying distance, with particle size. No direct relationships were established. Multivariate analysis was then used to study any and all contributions of the variables to particle size. Minitab was used

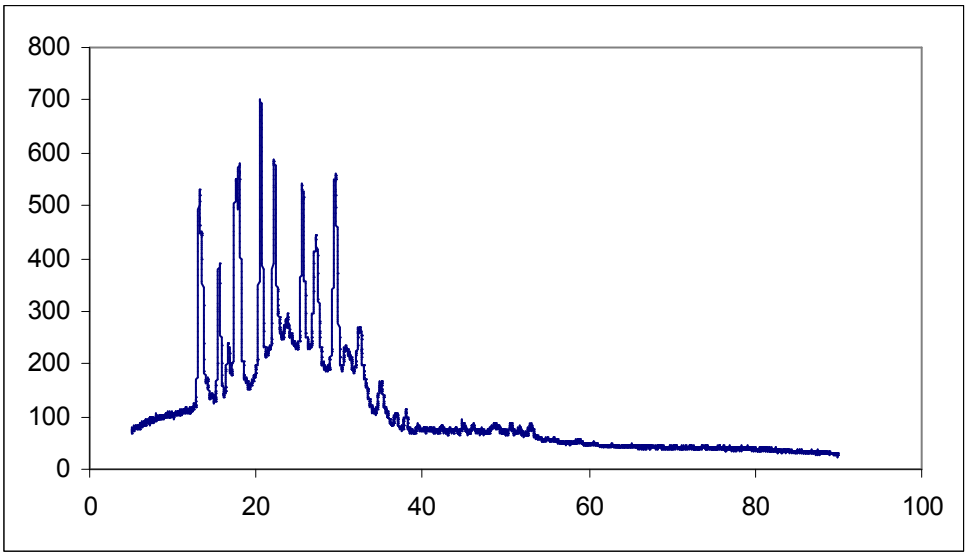

Figure 5.2: Raw X-ray Diffraction Spectrum of a 2 mg RDX film sprayed at rate of 2.5mL/hr, 4.128 cm from the substrate, with a carrier gas flow of 1293 mmHg.

to perform multiple linear regression and analysis of variance (ANOVA) on the data. The equation was determined to be:

$$d = 16.2 - 4.97\,a + 10.1\,b - 0.169\,c \quad (5.4)$$

d is particle diameter, a is concentration, b is spraying distance, and c is carrier gas flow. With an R^2 value of 77.1% and a p-value of 0, a correlation can be confirmed and a null hypothesis can be disregarded. The correlation would have been more significant had the R^2 value been greater. Flow rate and sample size appear to have been negligible variables. Although the R^2 value was a bit less than ideal for this equation, it was significantly greater than all other functions used to fit the data. All of this work, however, was preliminary and continues. Ideally, with more results, the R^2 value will increase closer to 100%.

References

[1]C. R. Siviour, M. J. Gifford, S. M. Walley, W. G. Proud, J. E. Field, Journal of Materials Science., **39**, 1255-1258 (2004)

[2]Behrens, R. (Private Communication)

[3]J. Akhavan, *The Chemistry of Explosives*, 2nd edition, Royal Society of Chemistry, 9-11, (2004).

[4]Fire and Explosions in the Canadian Upstream Oil and Gas Industry, WWW document, http://www.firesandexplosions.ca/index.php

Conclusion

Electrothermal chemical (ETC) ignition of propellants is new technology that has several important advantages over conventional ignition, most significantly, a reduced and highly reproducible ignition delay[1] and an ability to compensate bed temperature induced changes in muzzle velocity.[2] The interaction of the components in ETC ignition have been studied due to its advantages over conventional ignition. In ETC ignition, a piece of polyethylene replaces the primer, typically lead azide or black powder, found in conventional ignition. The plastic is attached to a large capacitor and when the capacitor is discharged, a plasma is formed described as the ETC igniter pulse. The ETC igniter pulse, which has been calculated to have pressures as high as 33 MPa and temperatures as high as 30,000 K.[3] Under these extreme conditions, the entropy of dissociation becomes greater than any bond enthalpy allowing for the dissociation of atoms from molecules and valence electrons dissociates from atoms. Therefore, the polyethylene dissociates into ions, radicals, electrons, and light. To understand the mechanism by which these plasmas ignite RDX, the individual and synergistic effects of these components have been studied. Erosion rates of RDX films exposed to electron cyclotron resonance(ECR) plasmas have been measured under a variety of plasma conditions. Experiments were performed to understand the roles of light, electrons, hydrogen radicals, hydrogen ions, and argon ions as a non-reactive probe of the effect of ion energy/momentum, alone and in combination. The most significant erosion rate was found in hydrogen plasmas with high-energy(under -500V and greater bias) where the synergistic effect of hydrogen ions and radicals appeared to be the greatest contributor. There is an 8-fold increase in erosion rate from a

0 V applied bias, where predominantly hydrogen radicals attack the surface, to an 800 V applied bias, where hydrogen ions and radicals attack the surface. Also, a 30-fold increase in the erosion rate is observed when the ion energy is increased from −15 V to −800 V applied bias.

The roles of ions and radicals were investigated further through exposing RDX films to mixed hydrogen-argon plasmas. This was studied because it was initially believed that propellants exposed to plasma might behave like semiconductors. In semiconductor etching, Winters and Coburn[4] observed a synergistic effect between the ions and radicals, in which simultaneous exposure resulted in an etch rate ~8x greater than either acting alone. In the etching of silicon, the enhancement results from the higher diffusion rate of reactive species through the partially reacted layer which is thinned by physical erosion due to ion bombardment. If the erosion rate of propellants behaved like semiconductor etching, then the addition of argon to a hydrogen plasma should greatly enhance the erosion rate as the much more massive argon ion provides for more effective physical sputtering. This is not observed. The addition of argon actually reduces the erosion rate compared to that found in pure hydrogen plasmas.

As a result, a new mechanism for the interaction of the plasma and the RDX beginning with the implantation of hydrogen has been developed and described. In this model, subsurface chemistry similar to that found in plasma deposition of diamond films, i.e. the first step involving the abstraction of hydrogen from a carbon in the RDX ring begins the chemistry. In the second step, the electron left from the hydrogen abstraction, on the carbon, combines with an electron from the nitrogen-nitrogen bond to form a double bond between the carbon and nitrogen and release the nitro group as a second

product with the hydrogen molecule. The subsurface nitrogen dioxide and the hydrogen, trapped together, then react to form water and nitric oxide and releasing subsurface heat, and consequently, initiating ignition.

To test the roles of carbon atoms and ions in the plasma generated by ETC ignition, an apparatus was designed to obtain a sample of pure carbon atoms. Two water-cooled electrodes were inserted into a glass chamber under vacuum. Inserted into the electrodes were graphite rods placed into contact with one another. As a power source for a discharge, an arc welder was attached to the electrodes. When turned on, the welder produced a pure carbon arc between the two graphite rods.[5] Carbon atoms were allowed to freely travel down the tube at the bottom to be collected on a glass slide. Once turned on, a 9.9 mg sample of carbon was obtained under vacuum onto a glass slide. Although the basic design proved successful, the integration of the apparatus to the erosion studies was not attempted.

Using a nebulizing spray technique, RDX particle size was investigated using powder x-ray diffraction under a variety of conditions including sample size, concentration, flow rate, gas flow, and spraying distance. Sample size is the amount of RDX in mg, concentration is the amount of RDX dissolved in acetonitrile, flow rate is the rate at which the RDX exits the nozzle of the nebulizer, gas flow is the pressure of the carrier gas(nitrogen) for the nebulizer, and the spraying distance is the distance from the nebulizer nozzle to the substrate. The motivation of this work is to achieve the most favorable RDX particle size ratio that is essential to ignition.

Crystalline size of explosives affects their sensitivity. Pure HMX on the centimeter-scale can be impacted with a flyer-plate at a velocity known to ignite

composite powders and nothing happens, showing that it is greatly insensitive[6]. It is believed in the field that composite powders with two different size particles (displaying a 10:1 size ratio) are vital to ignition. A flyer-plate hits the propellant causing a shockwave to compress the composite powder. This then causes the particles' jagged corners to rub against each other and create friction. This friction leads to hot spot formation, which starts ignition. A nebulizer can achieve this optimal ratio simply by depositing a film of certain size and manipulating a few variables, depositing a film that is ten times larger or smaller.

The Scherrer Equation was used to obtain the particle size of RDX measured by x-ray diffraction. The weighted diameters of the RDX particles were determined to range from 3.1 to 7.4 nm depending on experimental conditions. Performing a multivariate analysis, using concentration, gas flow, and spraying distance as independent variables and particle size as the dependent variable, an equation was determined to account for the change in particle size for RDX. Flow rate and sample size appear to have been negligible variables. The equation was determined to be:

$$d = 16.2 - 4.97\,a + 10.1\,b - 0.169\,c \quad (1)$$

d is peak diameter, a is concentration, b is spraying distance, and c is carrier gas flow. With an R^2 value of 77.1% and a p-value of 0, a correlation can be confirmed and a null hypothesis can be disregarded. However, all of this work is preliminary and continues.

References

[1]A. Chaboki, S. Zelenak, and B. Isle, IEEE Trans. Magn. **33**, 284 (1997).

[2]H. K. Haak, P. Scaffers, T. H. G. G. Weise, and H. G. Wisken, IEEE Trans. Magn. **39**, 231 (1997).

[3] M. J. Nusca and W. R. Anderson, CPIA Publication 712(38th JANNAF Combustion Subcommittee Meeting, 279 (2002)

[4] J. W. Coburn and Harold F. Winters, J. Appl. Phys. **50**, 3189 (1979)

[5] P. B. Shevlin "The Preparation and Reaction of Atomic Carbon". In R. A. Abramovitch. *Reactive Intermediates,* New York: Plenum Press. **1**, 1 (1980).

[6] Behrens, R. (Private Communication)